*3680–3698* *Nucleic Acids Research, 2019, Vol. 47, No. 7* *Published online 1 February 2019*
*doi: 10.1093/nar/gkz047*

# Mitochondrial RNA granules are critically dependent on mtDNA replication factors Twinkle and mtSSB

**Fenna Hensen[1], Alisa Potter[1,†], Selma L. van Esveld[2,†], Aleix Tarrés-Solé[3,†], Arka Chakraborty[3], Maria Solà[3] and Johannes N. Spelbrink[1,*]**

[1]Radboud Center for Mitochondrial Medicine, Department of Paediatrics, Radboudumc, Nijmegen, The Netherlands, [2]Radboud Center for Mitochondrial Medicine & Center for Molecular and Biomolecular Informatics, Radboud Institute for Molecular Life Sciences, Radboudumc, Nijmegen, The Netherlands and [3]Structural MitoLab, Department of Structural Biology, "Maria de Maeztu" Unit of Excellence, Molecular Biology Institute Barcelona (IBMB-CSIC), Barcelona 08028, Spain

Received June 27, 2018; Revised January 16, 2019; Editorial Decision January 17, 2019; Accepted January 24, 2019

## ABSTRACT

**Newly synthesized mitochondrial RNA is concentrated in structures juxtaposed to nucleoids, called RNA granules, that have been implicated in mitochondrial RNA processing and ribosome biogenesis. Here we show that two classical mtDNA replication factors, the mtDNA helicase Twinkle and single-stranded DNA-binding protein mtSSB, contribute to RNA metabolism in mitochondria and to RNA granule biology. Twinkle colocalizes with both mitochondrial RNA granules and nucleoids, and it can serve as bait to greatly enrich established RNA granule proteins, such as G-rich sequence factor 1, GRSF1. Likewise, mtSSB also is not restricted to the nucleoids, and repression of either mtSSB or Twinkle alters mtRNA metabolism. Short-term Twinkle depletion greatly diminishes RNA granules but does not inhibit RNA synthesis or processing. Either mtSSB or GRSF1 depletion results in RNA processing defects, accumulation of mtRNA breakdown products as well as increased levels of dsRNA and RNA:DNA hybrids. In particular, the processing and degradation defects become more pronounced with both proteins depleted. These findings suggest that Twinkle is essential for RNA organization in granules, and that mtSSB is involved in the recently proposed GRSF1-mtRNA degradosome pathway, a route suggested to be particularly aimed at degradation of G-quadruplex prone long non-coding mtRNAs.**

## INTRODUCTION

Human mitochondrial DNA (mtDNA) codes for a very limited set of 13 proteins, all of which are essential subunits of four of the five oxidative phosphorylation protein complexes. Their synthesis within the mitochondrial compartment is an absolute prerequisite for normal cellular ATP production. The maintenance of mtDNA integrity and copy-number, and a functional mitochondrial gene expression system are therefore essential for cell viability and require the coordinated action of several hundred nuclear encoded gene products, which are imported into the organelle. These include proteins involved in mtDNA replication and repair, all mitochondrial ribosomal proteins, RNA modification and homeostasis enzymes as well as structural proteins involved in the mtDNA/RNA compartmentalized organization.

MtDNA is organized in discrete DNA–protein complexes called nucleoids, which vary in their composition depending on their functional requirements and activity. For example, only a subset of nucleoids appears positive for the mtDNA replicative helicase Twinkle, mtSSB, or the polymerase γ accessory subunit POLG2 (1,2), indicating a specific commitment of these nucleoids to mtDNA replication. Noteworthy, there is a second nucleic acid-containing structure, termed the mitochondrial RNA (mtRNA) granule (3,4). RNA granules contain *de novo* synthesized mitochondrial RNA and are found either in close association with nucleoids or separated as discrete structures. In addition, RNA granules occasionally co-localize with RNA breakdown complexes termed RNA degradosomes (5). The exact function of RNA granules has not yet been resolved. Nonetheless, various associated proteins have been identified and characterized. These include enzymes involved in the initial processing of the polycistronic mitochondrial transcripts, such as RNaseP and Z, RNA ribonucleoside

*To whom correspondence should be addressed. Tel: +31 24 36 15191; Fax: +31 24 36 18900; Email: hans.spelbrink@radboudumc.nl
†The authors wish it to be known that, in their opinion, the second, third and fourth authors should be regarded as Joint Second Authors.
Present address: Arka Chakraborty, MRC Laboratory of Molecular Biology, Francis Crick Avenue, Cambridge, Biomedical Campus, Cambridge CB2 0QH, UK.

modifying enzymes and ribosome assembly factors (see e.g. (6)). Among them it is worth to mention the G-rich sequence factor 1 (GRSF1), which is involved in RNA processing and is commonly used as an immunofluorescence (IF) RNA granule marker. GRSF1 IF complements BrU labeling. The latter is used for *de novo* RNA synthesis detection and likewise highlights RNA granules (7). BrU labeling and GRSF1 IF typically show excellent co-localization. By manipulation of RNA granule proteins, several functions have been inferred for these RNA structures. However, it is unclear whether they are mostly RNA transit stations, main centers to organize mitochondrial gene expression to the point of mRNA translation, or have an undiscovered different primary function. So far, important questions are still open, such as whether most mtRNAs have a life beyond RNA granules, or whether these structures are the starting and end-point of most mtRNAs. In addition, related to this question, it is currently not clear if all *de novo* synthesized RNA is first found in the granule, irrespective of its final fate.

In this paper, we expand the list of proteins that are important for RNA granule biology. Surprisingly, these proteins are the well-known mtDNA replication factors Twinkle and mtSSB. We show that short-term depletion of these factors has clear and distinct RNA granule related phenotypes that alter our view of RNA granule function and establish the functional involvement of these proteins in granule formation and mtRNA processing/degradation. Our results provide additional insight into the function of RNA granules and associated proteins.

## MATERIALS AND METHODS

### Cell culture

HEK293 (ATCC CRL-1573), HEK293 Flp-In T-Rex cells (Invitrogen), U2OS cells (University of Helsinki, Finland) and in-house primary human fibroblasts were grown in Dulbecco's modified Eagle's medium (DMEM; Lonza BE12–604F) supplemented with 10% fetal calf serum (FCS) (GE Healthcare), in a 37°C incubator at 5% $CO_2$. All cell lines were routinely tested for mycoplasma contamination and found to be negative.

### Twinkle-bioID purification and mass spectrometric analysis

Bio ID pull downs were performed as described before with minor adjustments (8). Twinkle-bioID expressing and control cells (generated from Flp-In T-Rex 293 cell line, Invitrogen) were induced with 3 ng/ml AnhydroTetracyclin (AnTET, Sigma-Aldrich) for 24 h, washed and 3 h after AnTET removal treated with medium containing 50 μM biotin (Sigma-Aldrich) for 24 h. Cells were collected in PBS and 10 mg total protein was resuspended in 1.8 ml lysis-buffer (50 mM Tris–HCl pH 7.4, 500 mM NaCl, 0.4% SDS, 1 mM DTT), cells were fully lysed by the addition of 180 μl 20% Triton-X100 (TX100) and two rounds of sonication on ice (15 pulses; 1' ON, 3' OFF with 50% power) followed by the addition of 1.62 ml pre-chilled 50 mM Tris–HCl pH 7.8 and by another round of sonication. Cell debris was collected by centrifugation at 16 500 g for 10 min at +4°C. The supernatant was incubated with 100 μl Dynabeads MyOne Streptavidin C1 beads (Invitrogen) o/n at +4°C. Beads were washed as described by Roux *et al*. (8) and the samples prepared for mass spectrometric analysis by on-beads digestion. First, beads are resuspended in 50 mM ammonium bicarbonate (ABC) and 8 M Urea, and samples reduced with 10 mM dithiothreitol (30min at RT) and alkylated with 50 mM chloroacetamide (20 min at RT in the dark) before initial digestion by the addition of 1 μg LysC (Wako). After dilution with 8× ABC, the samples were subjected to tryptic digestion by the addition of 1 μg sequencing grade modified trypsin (Promega) o/n at 37°C while shaking. Peptide samples were desalted and concentrated by 'Stop And Go Extraction (STAGE) tips' (9) and the peptide sample was further purified by Pierce Detergent Removal Spin Columns (Thermo Scientific) before an injection of 28% of the sample in triplicate in the mass spectrometer.

Mass spectrometry measurements were performed by nanoLC 1000 (Thermo Scientific) chromatography coupled online to a Q Exactive hybrid quadrupole-Orbitrap mass spectrometer (Thermo Scientific). Chromatography was performed with an Acclaim PepMap 0.3 × 5 mm 5 μm 100 Å trap column (Thermo scientific) in combination with a 15 cm long × 100 μm ID fused silica electrospray emitter (New Objective, PicoTip Emitter, FS360–100-8-N-5-C15) packed in-house with ReproSil-Pur C18-AQ 3 μm 140Å resin (Dr Maisch, GMBH) (10). Tryptic peptides were loaded onto the trap column using 0.1% formic acid and separated by a linear 30 min gradient of 5–35% acetonitril containing 0.1% formic acid at a flow rate of 300 nl/min. The mass spectrometer was set to positive ion mode. Full MS events were performed at 70 000 resolving power (FWHM) at $m/z$ 200 using 1E6 ions or after 200 ms of maximal injection time. Data-dependent MS/MS spectra were performed using 1E5 ions at 17 500 resolving power (FWHM) at $m/z$ 200 or after 250 ms maximal injection time for the top 10 precursor ions with an isolation width of 3.0 Th and fragmented by higher energy collisional dissociation (HCD) with a normalized collision energy of 30%. Dynamic exclusion is set to 10.0 s.

Data analysis was performed with the MaxQuant software (version 1.5.0.25) (11) applying default settings with minor modifications. The precursor mass tolerance for Q Exactive measurements was set to 4.5 ppm. The multiplicity was set to 1 and trypsin was chosen as the proteolytic enzyme allowing for two miscleavages. Default MaxQuant normalizations were applied. Database searches were performed on the human UniProt database (release number 2016_11), in which the reversed database was used to calculate the false discovery rate (FDR), which was set to 1%. Isoleucine and leucine were forced to be treated equally. Between samples the option 'Match between runs' was enabled to detect sequenced peptides that were not subjected to a sequencing event in other samples and Label Free Quantification (LFQ) calculation was applied. The ProteinGroups.txt output file was further analyzed with the Perseus software (version 1.6.1.1.) (12). The mean was calculated from the log (2) LFQ intensity values from the triplicate measurements when there was a positive LFQ value for at least two out of three measurements. To visualize statistically significant data, four biological repeat experiments of the Twinkle-bioID samples are plotted in a volcano plot (S0 = 0.1; FDR

= 0.05) against in total six controls including three controls of the same cell line but without the addition of biotin to the medium, two controls of a bioID pulldown performed on cell lines overexpressing a FLAG-tagged Twinkle protein (without a biotin ligase) and one pcDNA5 control cell line in which the cells were transfected with an empty plasmid and therefore that cell line is not overexpressing any protein.

*RNA-interference and overexpression.* For knockdown, cells were transfected in six-well plates (for IF) or 10 cm cell culture dishes (for biochemical fractionation experiments) with a mixture of three Stealth™ siRNA duplex oligonucleotides for each gene of interest, at a concentration of 10 nM each, using Lipofectamine™2000. As controls we used Stealth™ Universal negative controls at the same concentrations.

Transient transfections with plasmids for Twinkle variants used TransIT-LT1 transfection reagent (Mirus), using manufacturer's instructions.

### MtDNA copy-number determination

Total DNA from U2OS cells was isolated using the NucleoSpin Tissue DNA purification kit (MACHEREY-NAGEL GmbH & Co.) according to the company's protocol and eluted into 50 μl of elution buffer. The amount of mtDNA was determined in relation to that of nuclear DNA (nucDNA). Measurement was performed by quantitative real-time PCR-based analysis (qPCR) with two pairs of human-specific primers. One primer pair was designed for amplification of the cytochrome b gene (Cytb) encoded by mtDNA: forward primer 5′-GCCTGCCTGATCCTCC AAAT-3′, and reverse primer 5′-AAGGTAGCGGATGA TTCAGCC-3′. The second primer pair was designed for amplification of the amyloid precursor protein gene (APP) encoded by nucDNA: forward primer 5′-TTTTTGTGTG CTCTCCCAGGTCT-3′, and reverse primer 5′-TGGTCA CTGGTTGGTTGGC-3′. Each PCR reaction in a total volume of 20 μl contained 25 ng of purified total DNA, 2.5 mM of forward and reverse primers, 10 μl of 2× SYBR Green Master Mix (Bio Rad) and was measured in triplicate in Hard-Shell 96-Well PCR Plates (Bio Rad). The amplification program for both genes was run as follows: initial denaturation at 95°C for 10 min, 40 cycles of denaturation at 95°C for 15 s and primers annealing at 60°C for 60 s; fluorescent signal was accumulated by a CFX96 Real-Time System (Bio Rad). The absence of non-specific amplicons was confirmed by melting curve analysis.

Fold changes in the relative amount of mtDNA in the siRNA treated cells compared to the negative control were calculated by the $2^{-\Delta\Delta CT}$ method. $C_T$ values of technical repeats that varied by >0.3 units from the others were removed prior to analysis. The qPCR results from three biological repeats of knock-down experiment were used for statistical evaluation using GraphPad Prism 5.03 for a one sample *t*-test, comparing each sample mean with the control value which was set to 100%.

### Western blot analysis

Following siRNA mediated knockdown, U2OS cells were collected and lysed for 10 min on ice in lysis buffer (50 mM Tris–HCl pH 7.4, 150 mM NaCl, 1 mM EDTA, 1% TX-100 and 2.5 mM PMSF) followed by a centrifugation step of 14 000 × g for 5 min at 4°C. 60 μg of cellular lysates were separated by SDS-PAGE followed by western blotting onto a supported nitrocellulose membranes. Membranes were probed with antibodies against proteins of interest and HRP-conjugated secondary antibodies followed by ECL detection. ECL reactions were visualized with a ChemiDoc instrument (Bio Rad). Antibodies used for Western blot detection were mtSSB (Sigma, HPA002866); TFAM (kind gift of Dr R. Wiesner); Twinkle (mouse-monoclonal, kind gift from Prof. Anu Suomalainen-Wartiovaara; see also (1)); CoxII (Abcam, ab110258); PHB1 (Abcam, ab28172); MRPL3 (Abcam, ab39268); MRPS22 (ProteinTech, 10984-AP); MRPL49 (ProteinTech, 15542-AP), GRSF1 (Sigma, HPA036985), Suv3 (kind gift of Dr Roman Szczesny), Actin (Novusbio, NB600-532H).

### Immunofluorescence

For immunofluorescent detection cells were grown on coverslips in six-well plates. Cells were fixed using 3.3% paraformaldehyde (PFA) in cell culture medium for 15–25 min, washed 3x in PBS and permeabilized for 15 min with 0.5% Triton X-100 in PBS/10% FCS. Fixed cells were incubated with primary and secondary antibodies at the following concentrations in PBS/10%FCS for 1 h: Twinkle (1:50–100); mtSSB (1:100); GRSF1 (1:200); Br(d)U (Roche, 11170376001, mouse monoclonal, 1:50); DNA (Progen, 61014, Mouse monoclonal, IgM, 1:400); J2 against dsRNA (Scicons, 10010200, 1:200); S9.6 against RNA:DNA hybrid (Millipore, MABE1095, 1:100). Secondary goat-anti-rabbit IgG, goat-anti-mouse IgG, goat anti-chicken IgG and goat antimouse IgM were AlexaFluor 488, 568, 633 and 647 (Invitrogen) labeled and used in various combinations at a 1:1000 dilution. Slides were mounted using ProLong® Gold antifade with DAPI (Invitrogen). Image acquisition used the Zeiss apotome system in apotome mode on an axio-observer Z.1 with Colibri led illumination and appropriate emission filters. In all cases in which controls are compared with experimental manipulation of cells (e.g. using siRNA), images have been acquired with identical illumination and exposure settings and processed identically. Where needed, images were further processed using Photoshop to adjust brightness/contrast and size/resolution. To generate high contrast digitized images for better visualization of co-localization we used the Squassh plug-in (13) in Fiji (ImageJ) (14) with default settings.

### Northern blot analysis

RNA was isolated from treated and control U2OS cells by TRIzol (Invitrogen) extraction according to manufacturers guidelines and 5 μg RNA was loaded on a 1.2% formaldehyde-agarose gel (1.2% agarose (Seakem® GTG™ agarose, Lonza) in 30 ml 5× formaldehyde running buffer (0.1 M MOPS pH 7.0, 40 mM sodium acetate pH 7.0, 5 mM EDTA pH 8.0) and 26.8 ml 37% formaldehyde in a final volume of 150 ml. The gel was run for 4–5 h at 60 V. The samples for the gel run were prepared by the addition of 5 μg RNA in a volume of 4.5 μl in 15.5 μl RNA sample buffer mix (10 μl formamide, 3.5 μl 37% formaldehyde,

**Table 1.** Oligonucleotide sequences used for Northern blot probe synthesis

| Oligo Name | Sequence (5′ → 3′) | Range mtDNA | Probe length |
|---|---|---|---|
| hND5-F | CAG TCT CAG CCC TAC TCC AC | 13061–13647 | 587 |
| hND5-R | GAA GCG AGG TTG ACC TGT TAG | | |
| hND6-F | TCC TCC CGA ATC AAC CCT GAC | 14261–14623 | 363 |
| hND6-R | GGG GTT TTC TTC TAA GCC TTC | | |
| hCytB-F | GGC TCA CTC CTT GGC GCC T | 14846–15358 | 513 |
| hCytB-R | CCC GTT TCG TGC AAG AAT A | | |
| h12S-F | GGT TTG GTC CTA GCC TTT C | 652–1156 | 505 |
| h12S-R | GCT GTG GCT CGT AGT GTT C | | |
| h16S-F | GGT AGA GGC GAC AAA CCT ACC G | 1981–2496 | 516 |
| h16S-R | CAG GCG GGG TAA GAT TTG CCG AG | | |
| hND1-F | GGC CAA CCT CCT ACT CCT C | 3315–3846 | 532 |
| hND1-R | GGG TCA TGA TGG CAG GAG T | | |
| hCOXI-F | GGC GCA TGA GCT GGA GTC | 5970–6478 | 509 |
| hCOXI-R | GCT GTG ATT AGG ACG GAT C | | |
| hCOXII-F | ATG GCA CAT GCA GCG CAA G | 7586–8269 | 684 |
| hCOXII-R | CTA TAG GGT AAA TAC GGG CCC | | |
| h18S-F | CCG CGC TCT ACC TAC CTA CC | - | 482 |
| h18S-R | CTT GGA TGT GGT AGC CGT TT | | |

2.0 μl 5× formaldehyde running buffer) and denaturation at 65°C for 15 min. The denatured RNA samples were chilled on ice for 2 min and 2 μl RNA loading buffer (50% glycerol, 0.1 mM EDTA pH 8.0, 0.25% bromophenol blue, 0.25% xylene cyanol FF and 9.1 μg/ml EtBr in order to visualize 18S and 28S rRNA bands) was added. Samples were run alongside a DIG labeled DNA ladder (Roche, Cat No. 11 669 940 910) that was similarly denatured as the RNA samples. For northern blotting after electrophoresis, the gel was incubated in 0.05 M NaOH for 20 min while shaking at RT followed by a 2 min autoclaved MQ wash at RT and 30 min wash with 20× saline–sodium citrate (SSC) buffer (3 M NaCl, 0.3 M. sodium citrate pH7.0). Northern blotting was performed overnight in 6× SSC onto a positively charged Nylon membrane (Roche). The blot was cross-linked afterwards for 3 min at 120 mJ UV-light before probe hybridizations with DIG (digoxigenin) labeled probes according to Roche protocols. After probe hybridization the membrane was briefly washed with 2× SSC/0.1% SDS and 2× for 15 min at 65°C with 0.5× SSC/0.1% SDS. The incubations of the Northern blots to prepare for immunological detection are performed as described by the DIG Wash and Block Buffer Set manual (Roche, Cat. No. 11 585 762 001) with CSPD ready-to-use (Roche). DIG labeled probes were synthesized using PCR products as template, originally synthesized using human genomic DNA with the oligos described in Table 1. The DIG labeling reaction used the same oligos in combination with PCR DIG Probe Synthesis Kit (Roche Cat. No. 11 636 090 910) according to manufacturers guidelines. Where necessary blots were stripped in between probings using 2 × 20 min washes in 0.1% SSC/1%SDS at 80°C.

Quantification of the northern blot detections was performed with the Image Lab 5.2.1 software with the 18S DIG labeled signal used for data normalization. Statistical analysis of the three biological repeated knockdowns was performed using GraphPad Prism 5.03 for a one-sample *t*-test, comparing each sample with its own control which was set to 100%.

### MtSSB electrophoretic mobility shift assay

*Protein production.* Human mtSSB (aa 15–148, without MTS) was amplified by PCR and cloned into pCRI7a (15), which adds an N-terminal 6His-tag to the protein. Sequence verified mtSSB vector was used to transform the protein expression *Escherichia coli* BL21 pLysS strain, and a fresh colony was picked to grow a pre-culture of 5 ml LB until saturation. This was inoculated to a second 100 ml pre-culture, also grown until saturation. From this culture, aliquots of 20 ml were inoculated into 2000 ml flasks containing 500 ml of LB. These latter grew to OD 0.6, cooled with ice, and induced with 1 mM IPTG and grown for 16 h at 16°C. All (pre-) cultures were shaken at 220 rpm o.n. at 37°C. Cells were harvested at 4000 × g for 15 min, cryo-cooled in liquid nitrogen and stored at –80°C. Cells were resuspended in buffer containing 250 mM NaCl, 50 mM Tris–HCl pH 7, 25 μg/ml DNase and RNase, 15 μg/ml T4 lysozyme, 4 mM MgCl2, with EDTA-free protease inhibitors (Roche), and lysed by sonication 2 × 1 min (2 s on, 4 s off, 35% amplitude) with one 5 min pause. Lysates were centrifuged at 20 000 rpm for 30 min using a JA-20 rotor. The supernatant was injected into a Ni-NTA column (GE Healthcare) mounted on an Äkta Purifier (GE Healthcare) system, washed with 5 column volumes (c.v.) and eluted with a linear gradient from buffer A (250 mM NaCl, 50 mM Tris pH 7.5, 50 mM imidazole) to buffer B (same as A with 500 mM imidazole) in 20 c.v. Quality of protein fractions was assessed by SDS-PAGE and purest fractions pooled and concentrated to a final volume of 250 μl for gel filtration chromatography using a Superdex 75 10/300 column (GE Healthcare), pre-equilibrated with running buffer (50 mM Tris–HCl pH 7.5, 250 mM NaCl). The purity of the peak fractions was analyzed by SDS-PAGE. Samples were flash-frozen with liquid nitrogen and stored at –80°C in 20% glycerol.

*Electrophoretic mobility shift assay (EMSA).* Human mtSSB binding assays were carried out with 50 nM DNA or RNA probes labeled with Cy5 at the 5′ end (Sigma-Aldrich). Probes have the following sequences: RNA, AG AACCUGUUGAACAAAAGC; ssDNA, AGAACCTG TTGAACAAAAGC. Nucleic acids were incubated with the indicated concentrations of mtSSB in 10 μl reactions, containing 10 mM Tris–HCl pH 8.0, 50 mM NaCl and 5% glycerol, for 30 min at room temperature. To reach every protein concentration, serial protein dilutions were performed on ice in 250 mM NaCl and 50 mM Tris–HCl pH 8.0. Binding reactions were loaded on 10% polyacrylamide gels in 0.5× Tris-borate EDTA buffer and electrophoresis

was run at 11 V/cm at room temperature in a MiniVE apparatus (Hoeffer). Gels were digitalized in Typhoon 8600 at the appropriate mode for Cy5 visualization excitation 649 nm and emission 666 nm).

## RESULTS

### Twinkle BioID identifies RNA granule proteins

In the past, proteomics of nucleoid preparations identified many proteins with primary RNA metabolism function (16–20). Vice versa, mtDNA-interacting proteins have unexpectedly been identified in RNA directed proteomics, including TFAM and mtSSB (21,22). We recently applied mtRNA directed methods to specifically identify the mitochondrial poly(A) RNA binding proteome, which detected mtSSB as a likely RNA interacting protein (Cansız-Arda & van Esveld *et al*., manuscript in preparation). In addition, similar to Han *et al*. (23) we have used Twinkle in proximity labeling experiments, but in contrast to Han *et al*. we used BioID with a Twinkle biotin-ligase fusion protein, which biotinylates proteins in close proximity and allows for their purification and identification by mass-spectrometry (Figure 1 and Supplementary Table S1). We expected to identify proteins directly involved with mtDNA replication and nucleoids, but both the published dataset by Han *et al*. and our data showed several RNA granule associated proteins, in particular GRSF1 and the mitochondrial RNase P subunit 1 protein MRPP1 (TRMT10C in Figure 1), which were highly enriched. These results intriguingly suggested an intimate link between RNA granules and nucleoids.

### Transient depletion of Twinkle or mtSSB has opposite RNA granule phenotypes and shows that Twinkle is essential for their formation

The suggested RNA binding activity of mtSSB and the detected connection between RNA granules and nucleoids led us to examine whether or not Twinkle and mtSSB have any direct involvement with RNA granules. Twinkle and mtSSB are well-characterized mtDNA replication factors, and their long-term depletion or knockout results in loss of mtDNA (24,25) and, consequently, loss of transcription templates. For this reason, all the experiments presented here concern the analysis after 68–72 h of siRNA-mediated knockdown. In addition to Twinkle and mtSSB, we also included GRSF1 depletion experiments and control experiments using non-targeting siRNA, as well as combined knockdowns indicated below. We analysed results by *in situ* bromouridine (BrU) RNA labeling and immunofluorescence, Western blot analysis, mtDNA copy-number determination and Northern blot analysis. All experiments used U2OS osteosarcoma cells, as we have shown previously that these show good knockdown efficiency. More importantly, we have shown by immunofluorescence after knockdown that there is little mosaicism (e.g. (1)), meaning that, in our hands, typically more than 99% of cells show a clear knockdown of the targeted protein.

Of the various knockdown experiments, Twinkle and combined Twinkle/mtSSB knockdown cells showed the strongest reduction of mtDNA copy number, by an ∼55–60% decrease as compared to control siRNA treated cells (Figure 2). MtSSB knockdown showed a modest reduction that was not statistically significant while GRSF1 knockdown showed an even smaller reduction that was however significant. Combined Twinkle/GRSF1 or mtSSB/GRSF1 knockdowns showed the same tendency as the individual Twinkle and mtSSB knockdowns. Overall, short-term knockdown of Twinkle, mtSSB or GRSF1 did not show a level of depletion of mtDNA to the extent that it would be expected to abolish mitochondrial transcription, and indeed Northern blot analysis also confirms this (see below and Figure 7).

Next, we examined *in situ* and *de novo* RNA synthesis using BrU labeling as well as immunofluorescent detection of the various proteins under study, following knockdown of Twinkle, mtSSB or GRSF1, and including combined knockdowns of these proteins (Figures 3–6 show 20 × 30 μm details; for full image fields for Figures 3–5 see Supplementary Figures S1–S3). In the course of these experiments, it became clear that GRSF1 is an excellent marker not just for RNA granules but also for the localization of all newly synthesized mitochondrial RNA, since GRSF1 at all instances showed similar localization and accumulation as BrU. Thus, following either BrU or GRSF1 IF gave us extra flexibility in the combined detection of proteins and newly synthesized mtRNA, and extra controls for consistency between experiments. In agreement with previously published results (3) (see also Discussion), GRSF1 knockdown showed an overall reduced intensity of BrU labeling, and thus reduced intensity of RNA granules (Figures 3 and 4). All experiments showed that *de novo* synthesized RNA, based on the BrU signal, was clearly present in RNA granules, but also appeared as an interstitial (uniform, non-granule) signal in varying degrees, depending on the protein that was depleted (see below). The presence of interstitial BrU signal indicated that not all *de novo* synthesized RNA is localized to RNA granules, or has a very short granule retention time (see also below and Discussion).

We examined the various knockdowns with BrU labeling in combination with either mtSSB (Figure 3), or GRSF1 antibody staining (Figure 4), or without BrU labeling but combining Twinkle and GRSF1 antibody staining (Figure 5). Our previously published experiments have shown that a Twinkle knockdown has a clear mtSSB phenotype, i.e. resulted in loss of mtSSB punctae and abrogation of mtDNA replication (1). The loss of mtSSB foci due to Twinkle knockdown was clearly reproduced here (Figure 3 and Supplementary Figure S1). Surprisingly, concomitant with a Twinkle decrease, RNA granules were also decreased while interstitial BrU signal was not affected and often increased, thus showing that the effect of Twinkle is not the consequence of lack of RNA synthesis. This is also clearly illustrated in Figure 4, in which we present the various siRNA combinations together with BrU and GRSF1 antibody labeling. The results show that in addition to an increased BrU interstitial RNA signal, also the GRSF1 interstitial signal was increased, further supporting that depletion of Twinkle results in increased interstitial RNA. At the same time, in Figures 3 and 4, considerably fewer bright foci, as signatures for RNA granules, were seen after Twinkle knockdown. Figure 5 presents Twinkle and GRSF1 antibody staining, and it clearly illustrates the same phenotype

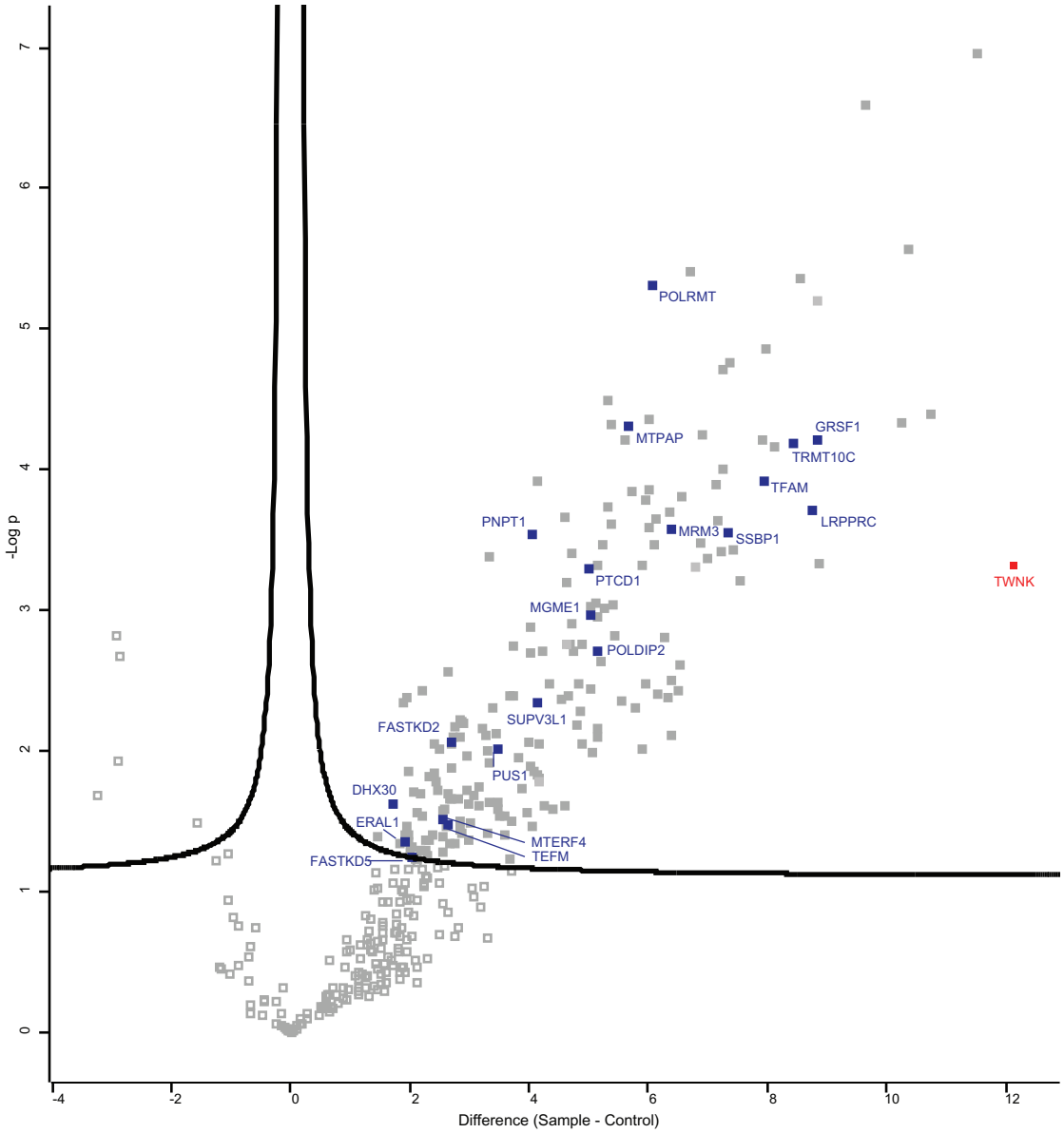


**Figure 1.** Twinkle BioID shows more than 8-fold enrichment for GRSF1 and MRPP1. Volcano plot showing statistically significant detected proteins (visualized in filled grey squares) in a Twinkle-bioID purification ($n = 4$) compared to control pull downs. Controls which are used include pull downs on the same cell line but without the addition of biotin to the medium ($n = 3$); pull downs performed on cell lines overexpressing a FLAG-tagged Twinkle protein (without a biotin ligase) ($n = 2$); and a pcDNA5 control cell line in which the cells were transfected with an empty plasmid and therefore that cell line is not overexpressing any protein ($n = 1$). These six controls all showed a very similar outcome and were therefore treated identically for the statistical analysis. The red square represents the position of the Twinkle protein (TWNK) in these pull downs and the blue squares represents a subset of well characterized RNA binding proteins as well as proteins involved in mtDNA maintenance which are statistically significantly enriched in Twinkle-bioID pull downs (the mitochondrial ribonuclease P protein1 or MRPP1 is indicated with its official symbol TRMT10C). The detailed results of the mass spectrometry results are given in Supplementary Table S1.

whilst in this case directly showing Twinkle knockdown efficiency.

In contrast to Twinkle, mtSSB knockdown had an opposite effect both on BrU and GRSF1, showing more and sometimes brighter RNA granules, with less interstitial RNA. This difference is particularly visible for GRSF1 staining in Figure 5, which shows the combined Twinkle and GRSF1 signals. It is important to emphasize that the experiments of Figures 3–6 always show parallel processed slides so that the individual knockdowns in each of these figures had the same processing, same antibody dilutions etc, and thus are directly comparable. Therefore, in particular the interstitial RNA signal intensities between the different experiments, either with BrU or with GRSF1, showed some

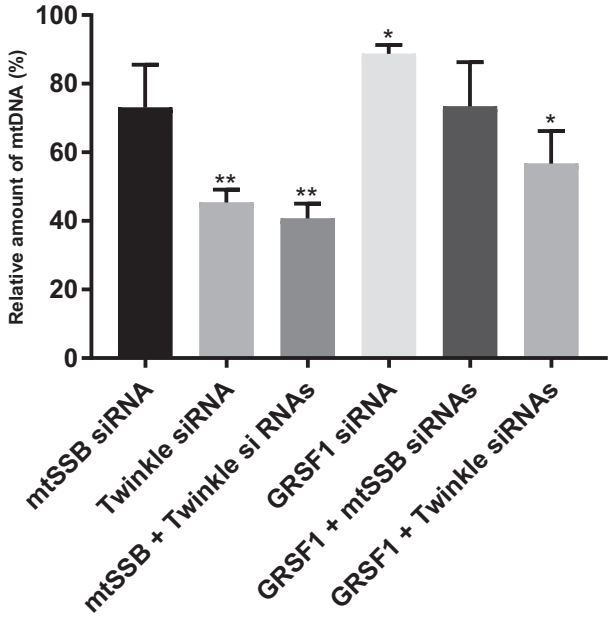


**Figure 2.** Short, 3-day knockdown of Twinkle, mtSSB and GRSF1 does not fully deplete mtDNA copy-number. Because the primary interest of this paper was the possible link between RNA granules and mtDNA replication factors Twinkle and mtSSB, we had to make sure that knockdown of these proteins would not completely deplete mtDNA copy-number as that would also severely affect mtRNA synthesis. For this reason, we tested a short 68–72 h knockdown of Twinkle, mtSSB, GRSF1 and combinations thereof in three biological repeats in U2OS cells, isolated total cellular DNA and measured copy number using qPCR. Results are presented as relative copy-number compared to control cells treated in parallel with non-targeting siRNA. Error bars show +/- SEM. Statistics used one sample *t*-test compared each sample to its own control that was set at 100. * indicates a *P*-value ≤ 0.05; ** indicates a *P*-value ≤ 0.01. Results show that indeed the effect of a 3-day knockdown of the various proteins and their combinations did not result in a severe loss of mtDNA. In all subsequent experiments we therefore used a 68–72 h knockdown regime.

variation, but within each experimental set the differences between control, mtSSB, Twinkle and GRSF1 were always clear and consistent.

We have previously shown that in, for example, human fibroblasts approximately 50% of nucleoids (based on DNA antibody staining) show co-localization with Twinkle foci. Of these, a much smaller percentage shows direct mtDNA replication activity (1). We show here that in Twinkle knockdown, GRSF1 RNA-granule foci diminished. And the converse too, in GRSF1 knockdown, bright 'nucleoid' Twinkle foci also disappeared (Figure 5). What is more, the control as well as the mtSSB knockdown clearly showed that a large proportion of Twinkle foci co-localized with GRSF1, explaining why approximately half of all nucleoids in a cell shows Twinkle juxtaposition but a much smaller percentage of nucleoids is actively replicating (1). These results thus show that juxtaposed Twinkle is otherwise involved and is present in RNA granules, validating the aforementioned Twinkle proximity labeling results, and the strong interdependence of Twinkle and GRSF1 in RNA granule formation. Double GRSF1/Twinkle knockdowns further confirmed these results as they showed the poorest RNA granule labeling using BrU (Figure 3 and 4). In contrast, GRSF1/mtSSB double knockdowns, showed some recovery of RNA granule BrU labeling compared to GRSF1 knockdown alone (Figure 3 and 4). This conforms with single mtSSB knockdown experiments that showed more BrU-intense RNA granules, compared to control and again suggests an opposite effect of Twinkle and mtSSB.

Importantly, Jourdain *et al.* (4) have shown, using our Twinkle-EGFP construct (26), very little Twinkle co-localization with RNA granules, which seems to contradict our findings. We have reproduced these experiments and confirm their observations, showing very little co-localization of overexpressed Twinkle-EGFP and endogenous GRSF1 (Supplementary Figure 4A). However, EGFP is not only a large protein tag of nearly 30 kDa, it also has the tendency to dimerize (27), which might interfere with the function of the protein it is attached to. In addition, Twinkle forms hexamers and heptamers, which further adds to the complexity of this specific protein fusion (28,29). For this reason, we also tested untagged and MycHis tagged versions of the protein to examine their co-localization with RNA granules. Both these versions showed important co-localization with endogenous GRSF1. In addition, Twinkle-FLAG-BirA, as used for the Twinkle BioID, also showed frequent GRSF1 co-localization (Supplementary Figure S4b). It furthermore showed persistent mtSSB puntae, indicative of functional mtDNA replication (Supplementary Figure S4c), and normal DNA antibody staining. All overexpressed Twinkle variants showed 100% co-localization with mtDNA (as shown for the Twinkle-FLAG-BirA variant).

All experiments presented in Figures 3–5 were triple labeled, with the third antibody used to detect (mt)DNA. Results showed that none of the knockdown combinations had a dramatic effect on mtDNA nucleoids, except for the GRSF1/mtSSB double knockdown that showed frequent abnormal nucleoid morphology (clearly visible in Figure 3; see also Supplementary Figures), even though not all cells were equally affected. Twinkle knockdown clearly showed a sparser number of mtDNA foci, in agreement with mtDNA copy-number measurements. We, however, did not quantify IF images directly for the number of mtDNA foci since it is not of direct relevance for this paper.

MtSSB knockdown, as shown above, resulted in less interstitial BrU and GRSF1, while in a combined knockdown with GRSF1 it resulted in some recovery in BrU RNA granule labeling. Figure 6 shows that the same held true for a double Twinkle/mtSSB knockdown. While Twinkle knockdown alone resulted in loss of bright BrU and GRSF1 foci, together with an increase of interstitial BrU and GRSF1 (see Figure 3 to 5), a double Twinkle/mtSSB knockdown showed restored bright BrU and GRSF1 RNA granules.

### MtSSB has a role in mtRNA processing and acts synergistically with GRSF1

In order to further understand the roles of Twinkle and mtSSB in RNA granule biology and, in particular, their role in RNA metabolism, we used Northern blot analysis to examine steady-state transcript levels (Figure 7), and precursor and long non-coding (lnc or nc) RNA species. This analysis was done on three biological replicates and several

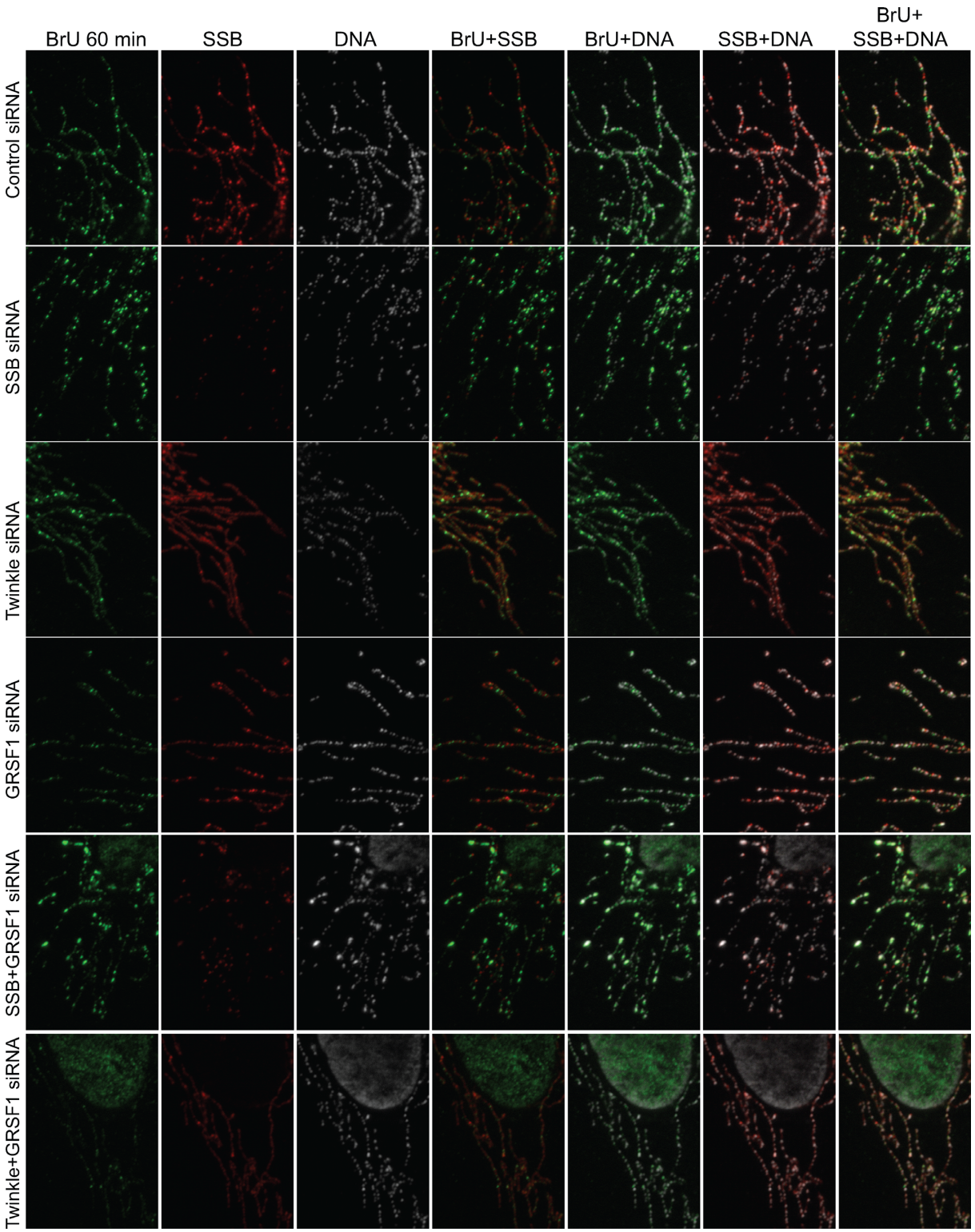


**Figure 3.** Twinkle and mtSSB depletion have distinct RNA granule phenotypes-1. U2OS cells were treated for 3 days with siRNAs for mtSSB, Twinkle, GRSF1, mtSSB+GRSF1, Twinkle+GRSF1 as well as universal control siRNAs, subsequently incubated for one hour with 2.5 mM BrU, briefly washed, fixed, lysed and incubated sequentially with a BrU, an mtSSB and a DNA antibody for immunofluorescent detection. Shown here are 20 × 30 μm representative details and including not only the individual antibodies but also the merged channel images, as indicated. Full images of the individual antibody detections are shown in Supplementary Figure S1. In addition, we show segmented high contrast images of the dual-channel overlay images of this Figure as a Supplementary Figure S7, having used the ImageJ Squassh plug-in ((13), see also M&M). This and subsequent Figures 4 and 5, for each figure, show parallel treated samples from a single six-well plate. The three knockdown experiments represented here in Figures 3–5 are thus biological repeats, albeit probed with different antibodies. For each individual Figure/experiment, all images were acquired with identical microscope settings, such as LED intensity, exposure time etc, and images were further processed identically. (See also Supplementary Figure S1 for full fields of view).

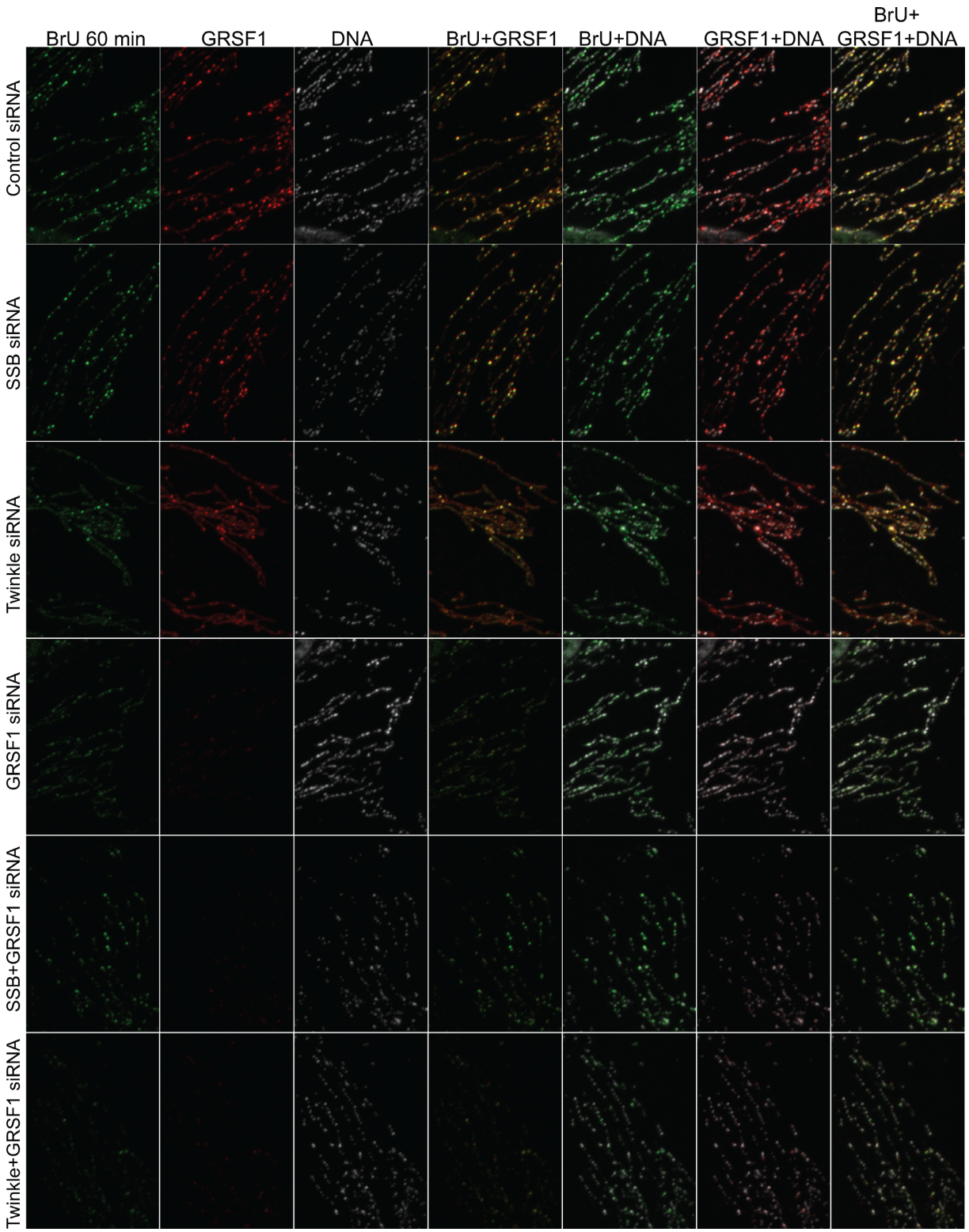


**Figure 4.** Twinkle and mtSSB depletion have distinct RNA granule phenotypes-2. Shown here is a repeat of the experiment in Figure 3, in this case with BrU labeling and detection and in addition GRSF1 and DNA antibody detection. (See also Supplementary Figure S2 for full fields of view).

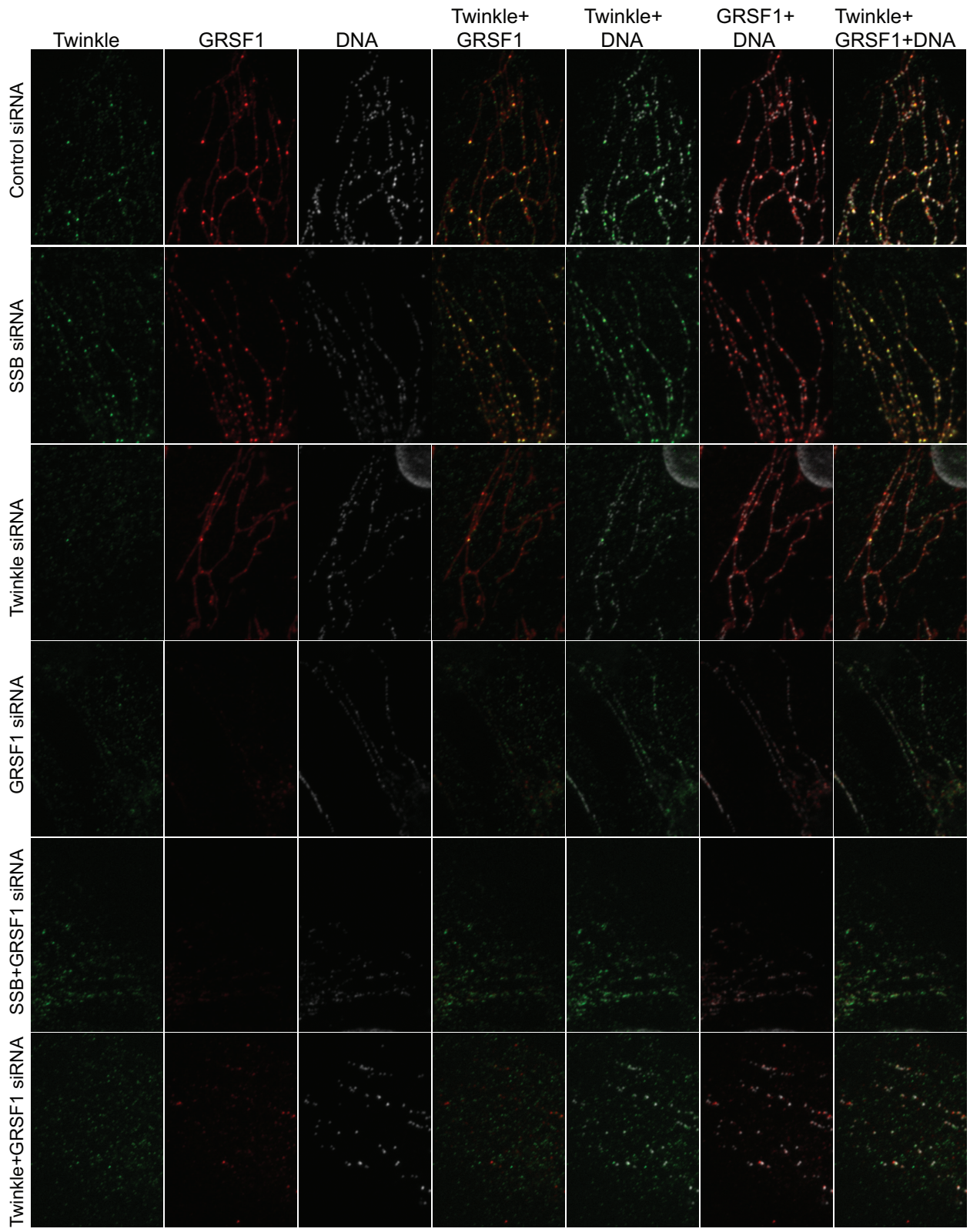


**Figure 5.** Twinkle and mtSSB depletion have distinct RNA granule phenotypes-3. Shown here is a repeat of the experiment in Figures 3 and 4, in this case with Twinkle, GRSF1 and DNA antibody detection. (See also Supplementary Figure S3 for full fields of view).

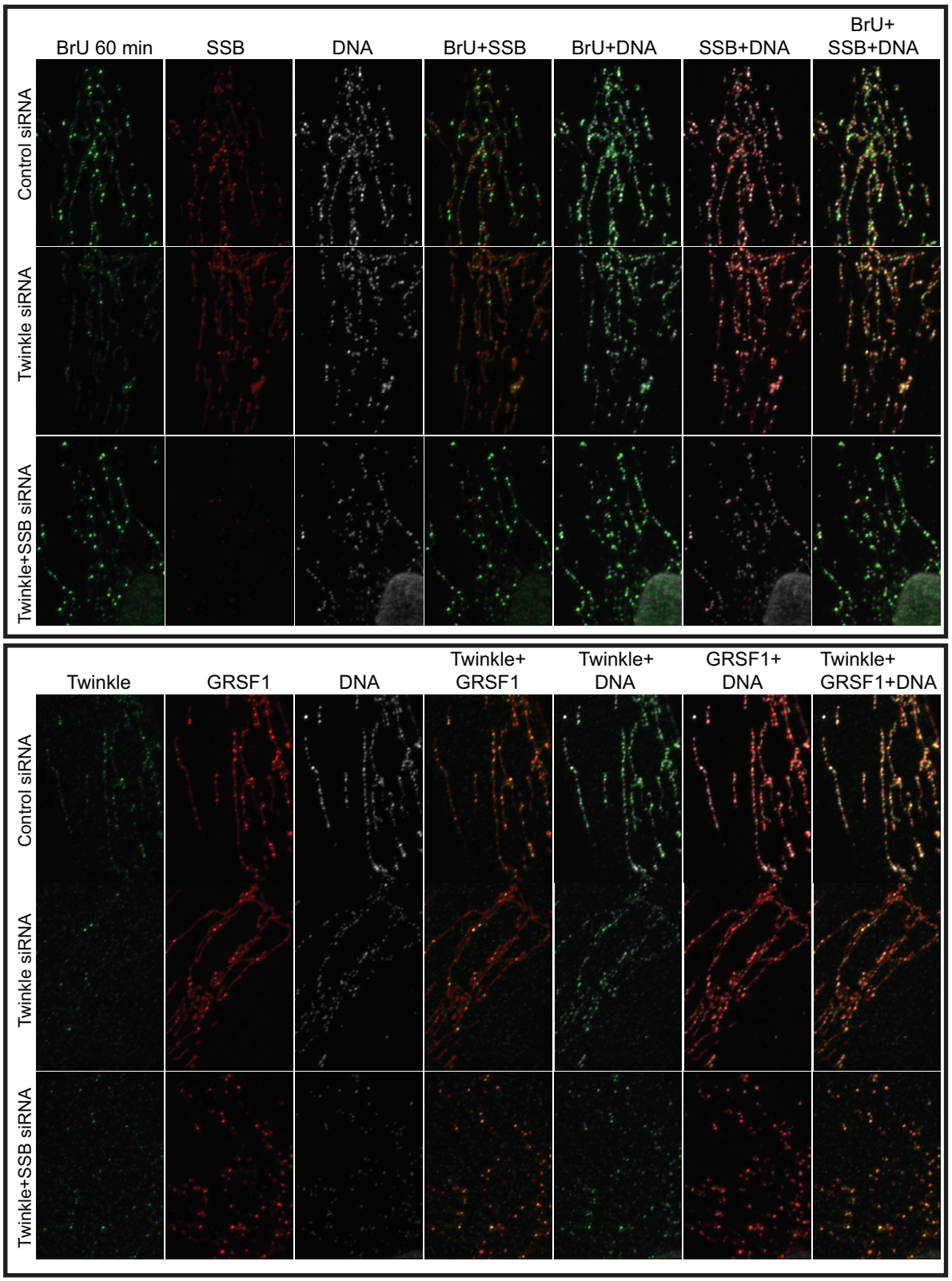


**Figure 6.** MtSSB depletion on top of Twinkle depletion restores RNA granules. U2OS cells were treated for 3 days with siRNAs for Twinkle and Twinkle+mtSSB as well as universal control siRNAs, and either (upper panel) or not (lower panel) incubated for one hour with 2.5 mM BrU. Upper panel, antibody incubations were for BrU, mtSSB and DNA, while for the lower panel Twinkle, GRSF1 and DNA antibodies have been used. Further details are as for Figures 3–5. Also in this case all treatments and processing has been done identical and in parallel.

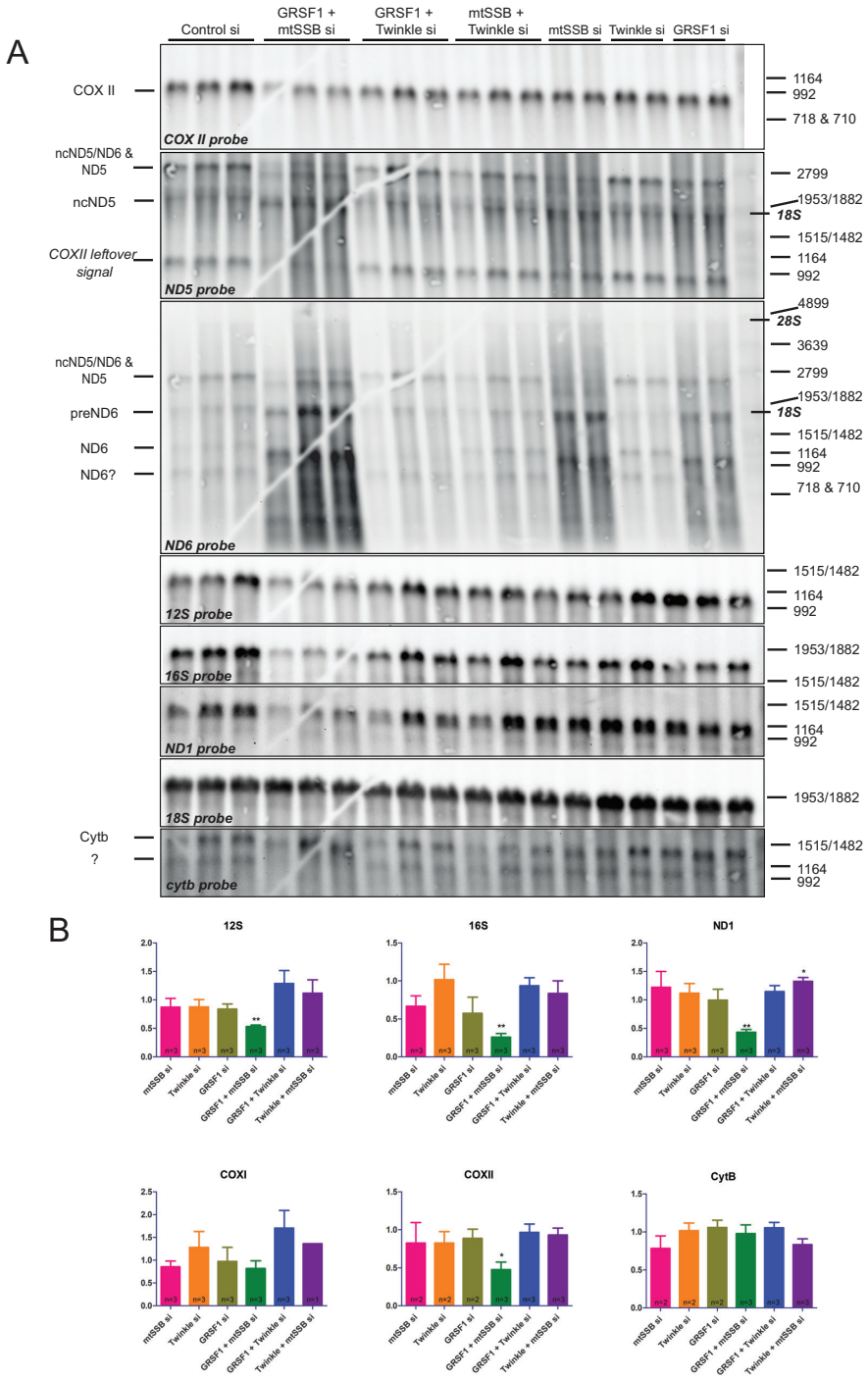


**Figure 7.** An mtSSB-GRSF1 double knockdown shows an exacerbated phenotype with rRNA depletion, RNA processing abnormalities and accumulation of degradation products. Northern blot analysis was done on three biological repeats and several technical variations to exclude gel and blot artifacts and to allow for the informed assignment of RNA species (see main text). (**A**) Images for the seven mitochondrial probes used here (*COXII, ND5, ND6, 12S* rRNA, *16S* rRNA, *ND1* and *CYTB*). A repeat blot on which the order of the *ND5* and *ND6* probe hybridizations was inverted and on which for example also the *COX1* probe was used (see quantification in **B**) is shown in Supplementary Figure S5. Markers show denatured commercial DIG labeled DNA markers (see M&M), that nonetheless are also good RNA size markers as shown by the localization of *18S* and *28S* rRNA (indicated in italic-bold on the right) in relation to the marker bands. Probe hybridizations were done in the order by which we show the panels, from top to bottom. For further information on the assignment of RNA species ,see the main text. RNA species are indicated by their generic names, and as either non-coding (nc) for the antisense RNA from the non-template strand or as precursor (pre). Quantification of signal after correction for *18S* ribosomal RNA as a loading control, used two blots for *12S*, *16S* and *ND1*, and one blot for the other probes (B). As for Figure 2, error bars show ± SEM. Statistics used one sample t-test comparing each sample to its own control that was set at 1 (not shown in the graphs). * indicates a *P*-value ≤ 0.05; ** indicates a *P*-value ≤ 0.01. Please note that the gel-crack that is visible on this particular Northern blot (A) occurred after the gel-run prior to blotting and thus has not affected the gel-run itself and is not a cause for the altered mobility of some RNA species.

technical variations using the same samples (gel runs with changed sample order and order of probe hybridizations) to exclude gel and blot artifacts and to allow for the informed assignment of RNA species. Based on these results and comparison with previous reports (3,4,30–33), in particular those dealing with mitochondrial lncRNAs covering the *CYTB-ND6-ND5* region, we came to the most likely assignment of fragments (as indicated in Figure 7A). A blot with the same samples loaded in different order and with a different order for some of the probe hybridizations, in particular the *ND5* and *ND6* probes, is shown in Supplementary Figure S5. The assignment of fragments was somewhat complicated by the fact that very few studies used size markers. The results (Figure 7A) show that both mtSSB and GRSF1 single knockdowns resulted in alterations in precursor and lncRNA species for *ND5*/*ND6* and a substantial accumulation of degradation products (visible as considerable background smearing). These alterations are not visible with other probes, thus showing that the samples are appropriately manipulated in all cases. Both knockdowns also showed a modest reduction in *12S* and *16S* rRNA levels that was not significant (Figure 7B), likely due to variation in knockdown efficiency. The above effects of the single mtSSB and GRSF1 knockdowns were however exacerbated in the double mtSSB/GRSF1 knockdown, resulting in significantly reduced *12S*/*16S* rRNA levels and the appearance/accumulation of RNA species that were otherwise not detected, while other species such as *ND1* and *COXII* were considerably reduced.

Western blot analysis of knockdown samples showed that concomitant with its effect on rRNA levels, a combined mtSSB/GRSF1 knockdown resulted in significantly reduced MRPL3/MRPL49 mitoribosomal protein levels, while in individual mtSSB and GRSF1 knockdowns MRPL3 was most clearly reduced, but only significant for the GRSF1 knockdown (Figure 8). These effects were also reflected in reduced COXII protein levels, both for the individual mtSSB and GRSF1 knockdowns as well as for the combined knockdown, but due to considerable variation between experiments, in particular for COXII, it just failed to reach statistical significance. This suggests and confirms a mitochondrial translation defect, as previously has been observed for a GRSF1 knockdown (3,4), that we expect would become more clearly visible with a longer knockdown. The Twinkle knockdown, which shows a larger reduction in mtDNA copy-number than mtSSB, GRSF1, or the combined mtSSB/GRSF1 knockdown, was unremarkable and comparable to control. This suggests, similar to all other results presented here, that mtDNA copy number was not a determining factor in the observed phenotypes. In contrast to the additive negative effects that were observed with the combined mtSSB/GRSF1 knockdown, the combined Twinkle/GRSF1 or Twinkle/mtSSB knockdown did not show clear additive effects.

Very recently, GRSF1 was shown to unwind RNAs able to form G-quadruplexes (G4) and facilitate degradosome-mediated degradation of lncRNAs that are G-rich and thus likely to form G4s (34). Almost simultaneously, it was shown that downregulation of the mitochondrial degradosome, consisting of the Suv3 helicase and the PNPase PNPT1 results in the accumulation of both dsRNA species as well as so-called R-loops, that are often transcription related RNA:DNA hybrids (35). Based on our results, in particular the accumulation of breakdown products detected with the *ND5* and *ND6* probes, in the GRSF1, mtSSB and their combined knockdowns, we sought a further confirmation for the suggestion that mtSSB would function in this same GRSF1-degradosome pathway. For this purpose we repeated knockdown experiments, now testing for either dsRNA, using the J2 monoclonal antibody (Figure 9), or for RNA:DNA hybrids using the monoclonal S9.6 antibody (Supplementary Figure S6). First of all, in a substantial fraction of control knockdown cells dsRNA is detected with the J2 antibody, albeit at low intensity. The S9.6 antibody on control cells shows a small percentage of cells (5–10%) with a clear mitochondrial RNA:DNA hybrid signal. Despite this mosaicism observed in control cells, knockdown of mtSSB, GRSF1 or their combined knockdown showed a consistent increase in signal for both dsRNA and RNA:DNA hybrid species (Figure 9 and (Supplementary Figure S6). In both cases, groups of cells with a failed knockdown are also visible highlighting the observed differences. These are indicated by –, or +/– for a partial knockdown and also in case of double knockdown where only one of the two proteins could be tested by co-staining and the knockdown status could therefore not be fully evaluated. Please also note that since the J2 and S9.6 antibodies are both mouse monoclonal they could only be used in combination with SSB or GRSF1 antibodies (both rabbit) and not with the Twinkle monoclonal antibody. As shown in Figures 3–6, these antibodies are however also diagnostic for a Twinkle knockdown. In contrast, in Twinkle and double Twinkle-mtSSB knockdowns either dsRNA or DNA:RNA hybrids were almost not detected. An additional observation was that in the different knockdown and antibody combinations, and in control cells, the majority of J2 and S9.6 antibodies foci co-localized with GRSF1 but not with mtSSB. This agrees with the earlier observations showing very little co-localization between BrU and mtSSB. Nonetheless, the similar effect of the mtSSB and GRSF1 knockdown on dsRNA and RNA:DNA hybrid accumulation suggest that mtSSB and GRSF1 both are active in the same mitochondrial lncRNAs degradosome pathway (see Discussion).

### MtSSB efficiently binds RNA

To further substantiate a proposed role for mtSSB in mitochondrial RNA metabolism, we purified human mtSSB and performed electrophoretic mobility shift assays by using 20 nt RNA or single-stranded DNA (ssDNA) probes, both labeled with Cy5 at the 5′-end. In agreement with the above results, at increasing concentrations of mtSSB, a shift of the RNA probe was observed. As expected, a band shift was also observed for ssDNA (Figure 10), but at lower mtSSB amounts, suggesting stronger binding than to RNA. Consistent with this, a close inspection of the localization of mtSSB, BrU and DNA in controls of Figures 3, 6 and Supplementary Figure S7 shows that, contrary to Twinkle and GRSF1, mtSSB appears more clearly in DNA foci than in the BrU ones. This and the above results indicate an important effect of mtSSB on RNA granules by a mechanism that

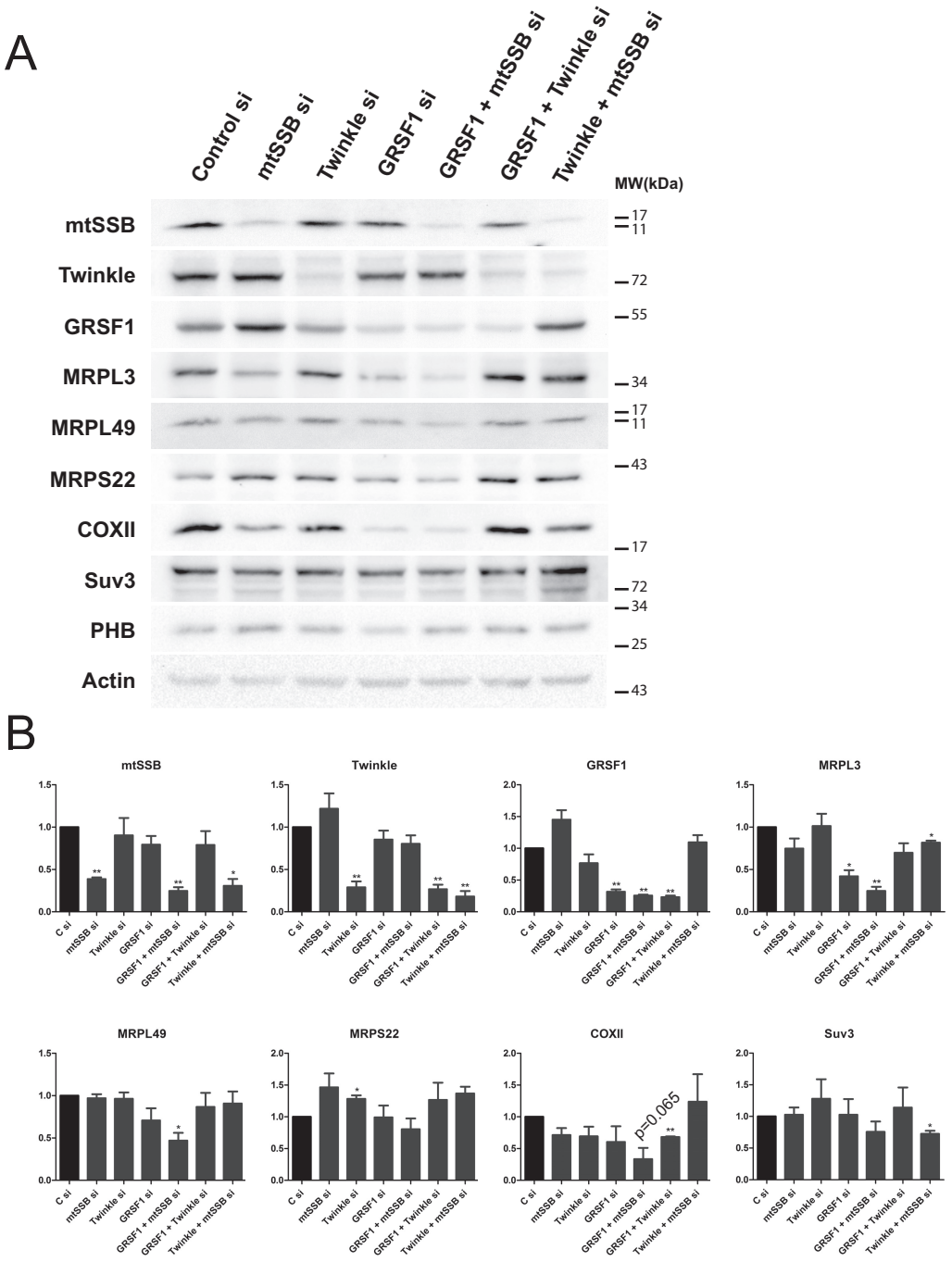


**Figure 8.** An mtSSB-GRSF1 double knockdown shows an exacerbated phenotype with reduced steady-state ribosomal protein levels and evidence of reduced mitochondrial protein synthesis. Total cellular lysates (60 μg) were prepared from the same knockdown experiments used also for DNA isolation, RNA isolation and Northern blot analysis as shown in Figure 7. A representative Western blot is shown and probed with Twinkle, mtSSB and GRSF1 antibodies to illustrate the effect of the knockdown of these proteins (**A**). In addition, several other relevant antibodies were used such as mitoribosomal antibodies (MRPL3, MRPL49 and MRPS22), COX II and Suv3, as well as a mitochondrial loading marker (prohibitin 1, PHB) and a cellular marker (Actin). (**B**) The quantification of three biological repeats on 3 Western blots, for which the band intensities were determined and corrected for loading based on the actin signal. As for Figure 2 and 7, error bars show ± SEM. Statistics used one sample *t*-test comparing each sample to its own control that was set at 1. * indicates a *P*-value ≤ 0.05; ** indicates a *P*-value ≤ 0.01. The *P* value for the COXII band in the combined mtSSB/GRSF1 knockdown is separately indicated, as it just failed to reach statistical significance despite it being consistently down.

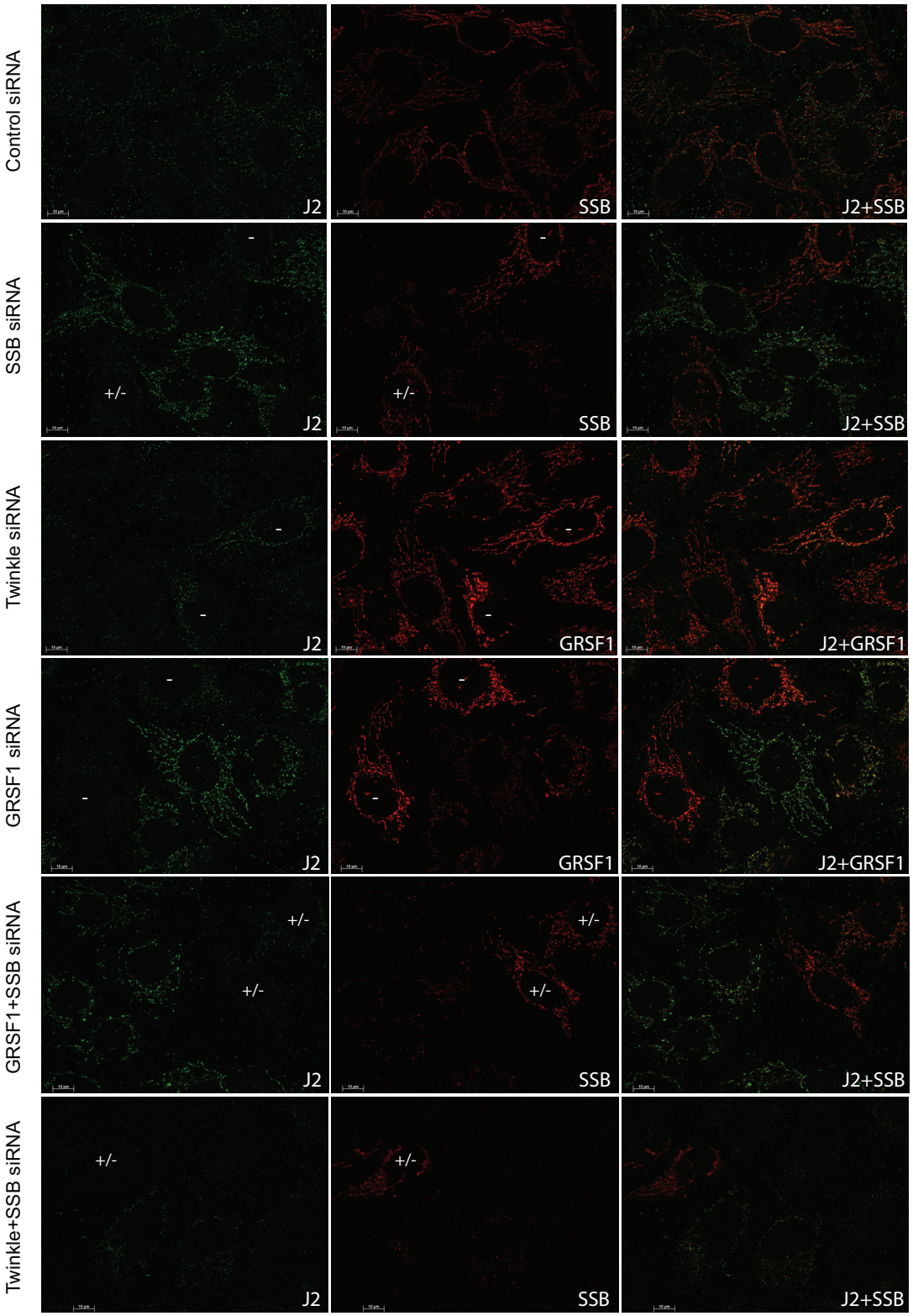


**Figure 9.** Both GRSF1 and mtSSB depletion result in dsRNA accumulation. U2OS cells were treated for 3 days with siRNAs for mtSSB, Twinkle, GRSF1, mtSSB+GRSF1, mtSSB+Twinkle as well as universal control siRNAs, and were sequentially processed and incubated with the J2 dsRNA (green), mtSSB or GRSF1 (red), and a DNA antibody (not shown) for immunofluorescent detection. Shown are the J2, and mtSSB or GRSF1 (as indicated) antibody incubations and their merged images. For all the targeted siRNAs, images were chosen in which also cells with failed knockdown are visible, as judged from the mtSSB/GRSF1 antibody incubations. These cells are indicated with either (–) for a failed knockdown or (+/–) to indicate either a partial knockdown or a failed double knockdown where at least one of the proteins was not depleted. For the Twinkle knockdown, the GRSF1 antibody incubation was used as a diagnostic antibody to determine knockdown, showing many more and more intense RNA granule-GRSF1 foci in those cells where the knockdown did not work properly. A similar experiment, but using the RNA:DNA hybrid antibody S9.6, is shown in Supplementary Figure S6.

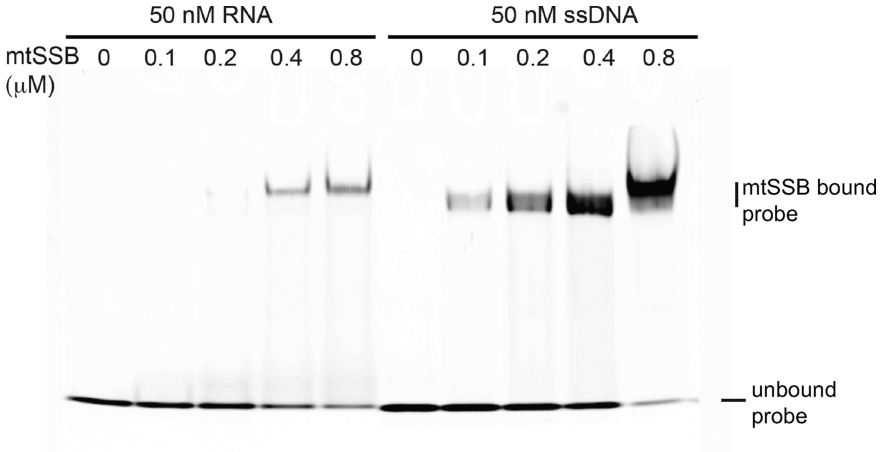


**Figure 10.** Purified human mtSSB efficiently binds RNA. EMSA of RNA and ssDNA (50 nM, 20 nt each) incubated at increasing concentrations of mtSSB is shown.

involves interstitial RNA binding, i.e. binding to RNA outside the confines of the mtRNA granule (see Discussion).

## DISCUSSION

In this paper, we have studied the interplay of mtDNA replication proteins, Twinkle and mtSSB, with mtRNA granules. This has led to a number of interesting findings that alter our view of mitochondrial RNA granule biology. The first surprising finding was the observation that the most prominent visible Twinkle foci that we previously have interpreted as Twinkle-nucleoid co-localization (1), also co-localized with GRSF1 foci. GRSF1 knockdown not only resulted in diminished RNA granule foci but also resulted in the disappearance of these Twinkle foci. Conversely, Twinkle depletion dramatically decreased RNA granules as visualized both by BrU labeling and GRSF1 immunofluorescence. However, in contrast to GRSF1 depletion, BrU incorporation in Twinkle knockdowns was still prominent but showed a mostly uniform, interstitial signal outside RNA granules, as also observed for GRSF1 as well as mtSSB signals. In contrast to Twinkle depletion, mtSSB depletion resulted in less interstitial RNA and GRSF1. Whereas GRSF1 depletion led to overall less BrU signal, a combined GRSF1/mtSSB knockdown at least partially restored RNA granule signal compared to GRSF1 depletion alone. This suggests that in the absence of GRSF1, RNA could still be released or further processed and/or degraded from granules. However, in combination with mtSSB depletion it could no longer do so, and thus accumulated at higher levels in granules. This interpretation is further corroborated by Northern blot analysis showing that both GRSF1 and mtSSB depletion showed a similar *ND6* precursor accumulation and the appearance of abnormally processed and poorly degraded transcripts, while the combined knockdown showed a cumulative effect. Likewise GRSF1, mtSSB as well as their combined depletion resulted in the accumulation of dsRNA and RNA:DNA hybrid R-loops. This suggests, also on the basis of two very recent papers ((34,35), see below) that mtSSB, apart from its single-stranded DNA-binding activity, functions in the pathway for degradation of G-rich lncRNAs as GRSF1.

Our results are the first to show that RNA transits to and from the RNA granules and has a function beyond them. A long retention time and accumulation of at least some newly synthesized RNA species could make RNA granules into visible entities. Twinkle depletion might strongly decrease the RNA retention time, without obvious effects on RNA processing. Twinkle depletion also results in disappearance of mtSSB nucleoid foci and shows a concomitant increase in interstitial mtSSB. We can therefore hypothesize that, in the absence of Twinkle, the reduced mtSSB nucleoid co-localization increases the availability of mtSSB, which stimulates lncRNA degradation and possibly also RNA processing and/or release of RNA from RNA granules. At this point, our results cannot exclude that Twinkle itself also plays a direct role in retention of RNA in granules given its prominent presence in granules and its disappearance from granules by GRSF1 depletion. However, the double Twinkle/mtSSB knockdown that shows a re-establishment of RNA granules suggest a primary role for mtSSB in degradation and/or release of RNA from granules.

Newly synthesized mtRNA was first observed to accumulate in discrete structures using BrU labeling (7). With the identification of the first protein to specifically co-localize with these structures, namely GRSF1, they were coined RNA granules (3,4). To this day, there is discussion whether or not RNA granules are to be considered separate from nucleoids. Based on the data we present here, we suggest they should be mostly considered as contiguous with nucleoids, although we cannot fully exclude there is a smaller sub-population that could become detached. Based on the images we present, in our hands the vast majority of granules partially or fully overlap with nucleoids. This is also illustrated in Supplementary Figure S7, in which we show segmented high contrast images of the dual-channel overlay images in Figure 3 using the ImageJ Squassh plug-in ((13) and see Materials and Methods). More importantly, bright GRSF1 foci that are considered diagnostic for RNA granules, show a near 100% co-localization with the mtDNA he-

licase Twinkle, that we have previously shown co-localizes with mtDNA (1).

The original two GRSF1/RNA granule publications proposed that these RNA entities are involved in nascent-chain RNA processing as well as mitoribosome biogenesis. However, there was no clear consensus of the actual functions of either GRSF1 or RNA granules. This was in part caused by contradictory results. For example Jourdain *et al*. (4) suggested that with a GRSF1 knockdown, BrU incorporation was normal and in fact persisted in granules during a chase. In contrast, Antonicka *et al*. (3) suggested that BrU foci by-and-large disappeared following a GRSF1 knockdown (although results were 'not shown'). In both papers, steady-state RNA levels were found to decrease following GRSF1 knockdown, which is consistent with a reduced BrU labeling as suggested by Antonicka *et al*. Similar to the observations by Antonicka *et al*. we consistently observed reduced BrU incorporation, which we contrasted with various complementary knockdown experiments done in parallel. In addition, in the combined GRSF1/Twinkle knockdown, BrU labeling was even more dramatically decreased. On Northern blot the GRSF1 and combined GRSF1/Twinkle knockdowns were not reflected in uniformly and dramatically reduced steady-state RNA levels, suggesting that stability was in fact increased, as observed by Jourdain *et al*. The observed differences in BrU labeling intensities in the knockdowns of these two reports (3,4) might be due to subtle differences in the corresponding approaches such as duration and efficiency of GRSF1 knockdown, cell lines used, cell culture confluence and so on. In addition, we should also consider the BrU detection itself. Similar to BrdU detection, in which a denaturation step is required to render at least partially single stranded DNA, BrU perhaps also needs to be present in a single-stranded conformation for it to be detected. Thus, if a treatment, such as GRSF1 depletion results in the accumulation dsRNA and RNA:DNA hybrids, those species might not always be detected efficiently without a denaturation step prior to antibody incubation.

A second point of contention between Antonicka *et al*. and Jourdain *et al*. is whether or not GRSF1 is involved in RNA processing. In addition, a recurrent arising question is whether granules are specific for certain RNA species, or all *de novo* synthesized RNA passes through granules. Our data clearly shows that not all mtRNA is present in RNA granules, as suggested by varying degrees of visible interstitial RNA following BrU labeling. Immunofluorescent detection of BrU labeled mtRNA can be misleading. As with any immunofluorescent detection, a focal concentration of epitope and antibody (irrespective of whether the antibody detects protein or nucleic acid) will result in intense punctate fluorescence that can be further emphasized by a high threshold for low intensity signals and high contrast settings. The majority of mtRNA, whether or not *de novo* synthesized, might in fact not be present in RNA granules, but since it is not concentrated but rather spread throughout the mitochondrial network can be more difficult to detect. An additional complication might be that RNA that is being packed or covered by protein might not be easily detectable by a BrU antibody and its concentration might be underestimated. For example, one could question whether BrU labeled rRNA that is fully assembled within the protein-rich mitoribosome would be detectable. The idea that not all mtRNAs pass through RNA granules is indirectly supported by GRSF1-RNA immunoprecipitation as well as by mitochondrial FISH detecting individual mitochondrial transcripts (3,31). Antonicka *et al*. showed that FISH probes that detect light-strand transcripts and cover *ND6* as well as lncRNAs for *CYTB* and *ND5,* are observed as punctate and co-localize with GRSF1 foci, whereas for example a *12S* RNA probe shows a much more uniform mitochondrial distribution. Likewise, Chatre and Ricchetti (36) (in particular Figure 2 of this publication) show that, by using FISH probes for most mitochondrial transcripts, in particular those probes that detect RNAs in the region of *ND5*, *ND6* and *CYTB*, have a punctate fluorescence reminiscent of RNA granules, while probes covering *16S* and *ND1* give a mostly uniform appearance. Somewhat at odds with the above findings is that Antonicka *et al*. (3) see little evidence for a processing defect that involves the *ND6* region, while in contrast Jourdain *et al*. (4) do see a processing defect for RNAs covering this region, although they also suggest a more widespread processing defect. More recent papers that examine various possible RNA granule proteins do see defects, in particular for the *ND6* region (31–33), although some proteins such as the FAST kinase domain protein 5 (FASTKD5) (31), give very specific RNA processing defects not involving the *ND6* gene region. However, based on published immunofluorescence detection of FASTKD2 and 5 (31) it appears that FASTKD2 is much more specific for RNA granules than FASTKD5 is, and it is FASTKD2 that, similar to GRSF1, gives an *ND6* RNA processing defect (33). Likewise, a mitochondrial variant of FASTK appears specific for RNA granules and again affects the *ND6* region RNAs (32). The emerging picture is that RNA granules are enriched particularly for light-strand transcripts covering the *ND6* gene region including lncRNA that are derived from that region (as originally proposed by Antonicka *et al*. (3)), or that those RNAs reside much longer in granules compared to most other mtRNAs. Very recently, this idea has been given new weight by Pietras *et al*. (34), who implicate GRSF1 very specifically in the degradosome mediated degradation of G-quadruplex (G4) containing lncRNAs, that are most prominently derived from the L-strand surrounding the *ND6* gene. It is striking that the Northern blots for our double mtSSB/GRSF1 knockdown (and to a lesser extend the single knockdowns for these 2 proteins) also resemble the degradosome-component PNPase and Suv3 knockdown results by Jourdain *et al*. (32). Combined with our immunofluorescence data and the suggested roles for PNPase, SUV3 and now also GRSF1, both in degradation of lncRNAs and *ND6* processing (5,32,37), we can suggest that when the lncRNAs and *ND6* RNA species are unable to exit the granule, they are not processed and/or degraded properly. Since mtSSB knockdown in many ways mimicks the GRSF1 knockdown, and the combined GRSF1/mtSSB knockdown shows an exacerbated phenotype with a promi-

nent accumulation of abnormally processed and poorly degraded RNA, we can firmly assign an additional function for mtSSB in assisting in the degradation of G4 lncRNAs. Pietras *et al*. (34) showed that GRSF1 likely functions to render G4 RNAs single-stranded so it becomes a better substrate for the Suv3/PNPase degradosome. Perhaps the role for mtSSB in this pathway is to bind unfolded RNAs following GRSF1 action and prevent it from reforming G-quadruplexes. Further experiments will be needed to test this hypothesis.

RNA granule enriched proteins, while having a clear role within the granule are likely to have roles outside granules as well. GRSF1 is a granule-resident protein but also gives interstitial signal. Immunoprecipitation of GRSF1 enriches for light-strand transcripts around *ND6* (31), but also enriches for many other transcripts including ribosomal RNAs. Thus, GRSF1 is perhaps also a rather generic RNA binding protein present both in and outside granules. Its knockdown effect on *12S*/*16S* rRNA might simply be a consequence of reduced rRNA stability or even synthesis, thereby affecting ribosomal assembly. The same could hold true for DEAD-box helicase 28 (DDX28) (31,38). If we accept a role for RNA granule enriched proteins outside the confines of RNA granules, then the concept that these structures are the primary sites of mitoribosomal assembly requires further experimental verification. While we do not contend that mitoribosomal assembly is at least in part taking place in close association with mtDNA nucleoids, as has been shown in elegant experiments by Bogenhagen *et al*. (19,39), also supported by Dalla Rosa *et al*. (40), and observed in yeast (41), we do challenge that the currently available data very clearly demonstrate that the sites for ribosomal assembly are mtRNA granules. In contrast, and even though one function does not exclude another function, mtRNA granule involvement with G4 prone lncRNAs seems very persuasive.

The roles of Twinkle and mtSSB beg the question if and how RNA granules might be of relevance to mtDNA replication. Vice versa, our results also have consequences for the interpretation of Twinkle associated disease mutations. For example, Twinkle mutations associated with Perrault syndrome (42), a disease mostly associated with factors that function in mitochondrial translation and protein quality control (43,44), might be interpreted in light of a mitochondrial RNA metabolism function of Twinkle.

## SUPPLEMENTARY DATA

Supplementary Data are available at NAR Online.

## ACKNOWLEDGEMENTS

We acknowledge Giorgio Medici and Helga van Rennes for laboratory support.

## FUNDING

Prinses Beatrix Spierfonds and the Stichting Spieren voor Spieren [W.OR15–05 to J.N.S.]; European Union's Horizon 2020 research and innovation programme under the Marie Sklodowska-Curie grant agreement [721757 to A.P.]; PhD fellowship from the Radboud Institute for Molecular Life Sciences; Radboudumc [R0002792 to S.LvE.]; Spanish Ministry of Economy and Competitiveness (MINECO) [BFU2015-70645-R to M.S.]; Ministry of Education, Culture and Sports [FPU14-06021 to A.T.-S.]; Generalitat de Catalunya [2017-SGR-1192 to M.S.]; European Union [FP7-HEALTH-2012-306029-2 to M.S.]; ITN Fellowship FP7-PEOPLE-2011-290246 to A.C.]; The Structural Biology Unit at IBMB-CSIC is a 'Maria de Maeztu' Unit of Excellence awarded by MINECO [MDM-2014-0435]. Funding for open access charge: Institutional and in part defrayed by the Prinses Beatrix Spierfonds and the Stichting Spieren voor Spieren [W.OR15–05].

*Conflict of interest statement.* None declared.

## REFERENCES

1. Rajala,N., Gerhold,J.M., Martinsson,P., Klymov,A. and Spelbrink,J.N. (2014) Replication factors transiently associate with mtDNA at the mitochondrial inner membrane to facilitate replication. *Nucleic Acids Res.*, **42**, 952–967.
2. Lewis,S.C., Uchiyama,L.F. and Nunnari,J. (2016) ER-mitochondria contacts couple mtDNA synthesis with mitochondrial division in human cells. *Science*,**353**, aaf5549.
3. Antonicka,H., Sasarman,F., Nishimura,T., Paupe,V. and Shoubridge,E.A. (2013) The mitochondrial RNA-binding protein GRSF1 localizes to RNA granules and is required for posttranscriptional mitochondrial gene expression. *Cell Metab.*, **17**, 386–398.
4. Jourdain,A.A., Koppen,M., Wydro,M., Rodley,C.D., Lightowlers,R.N., Chrzanowska-Lightowlers,Z.M. and Martinou,J.C. (2013) GRSF1 regulates RNA processing in mitochondrial RNA granules. *Cell Metab.*, **17**, 399–410.
5. Borowski,L.S., Dziembowski,A., Hejnowicz,M.S., Stepien,P.P. and Szczesny,R.J. (2013) Human mitochondrial RNA decay mediated by PNPase-hSuv3 complex takes place in distinct foci. *Nucleic Acids Res.*, **41**, 1223–1240.
6. Pearce,S.F., Rebelo-Guiomar,P., D'Souza,A.R., Powell,C.A., Van Haute,L. and Minczuk,M. (2017) Regulation of mammalian mitochondrial gene Expression: Recent advances. *Trends Biochem. Sci.*, **42**, 625–639.
7. Iborra,F.J., Kimura,H. and Cook,P.R. (2004) The functional organization of mitochondrial genomes in human cells. *BMC Biol.*, **2**, 9.
8. Roux,K.J., Kim,D.I. and Burke,B. (2013) BioID: a screen for protein-protein interactions. *Curr.Prot. Protein Sci.*, **74**, doi:10.1002/0471140864.ps1923s74.
9. Rappsilber,J., Ishihama,Y. and Mann,M. (2003) Stop and go extraction tips for matrix-assisted laser desorption/ionization, nanoelectrospray, and LC/MS sample pretreatment in proteomics. *Anal. Chem.*, **75**, 663–670.
10. Ishihama,Y., Rappsilber,J., Andersen,J.S. and Mann,M. (2002) Microcolumns with self-assembled particle frits for proteomics. *J Chromatogr A*, **979**, 233–239.
11. Cox,J. and Mann,M. (2008) MaxQuant enables high peptide identification rates, individualized p.p.b.-range mass accuracies and proteome-wide protein quantification. *Nat. Biotech.*, **26**, 1367–1372.
12. Tyanova,S., Temu,T., Sinitcyn,P., Carlson,A., Hein,M.Y., Geiger,T., Mann,M. and Cox,J. (2016) The Perseus computational platform for comprehensive analysis of (prote)omics data. *Nat. Methods*, **13**, 731–740.
13. Rizk,A., Paul,G., Incardona,P., Bugarski,M., Mansouri,M., Niemann,A., Ziegler,U., Berger,P. and Sbalzarini,I.F. (2014) Segmentation and quantification of subcellular structures in fluorescence microscopy images using Squassh. *Nat. Protoc.*, **9**, 586–596.
14. Schindelin,J., Arganda-Carreras,I., Frise,E., Kaynig,V., Longair,M., Pietzsch,T., Preibisch,S., Rueden,C., Saalfeld,S., Schmid,B. *et al.* (2012) Fiji: an open-source platform for biological-image analysis. *Nat. Methods*, **9**, 676–682.

15. Goulas,T., Cuppari,A., Garcia-Castellanos,R., Snipas,S., Glockshuber,R., Arolas,J.L. and Gomis-Ruth,F.X. (2014) The pCri System: a vector collection for recombinant protein expression and purification. *PLoS One*, **9**, e112643.
16. Wang,Y. and Bogenhagen,D.F. (2006) Human mitochondrial DNA nucleoids are linked to protein folding machinery and metabolic enzymes at the mitochondrial inner membrane. *J. Biol. Chem.*, **281**, 25791–25802.
17. Bogenhagen,D.F., Rousseau,D. and Burke,S. (2008) The layered structure of human mitochondrial DNA nucleoids. *J. Biol. Chem.*, **283**, 3665–3675.
18. Hensen,F., Cansiz,S., Gerhold,J.M. and Spelbrink,J.N. (2014) To be or not to be a nucleoid protein: A comparison of mass-spectrometry based approaches in the identification of potential mtDNA-nucleoid associated proteins. *Biochimie*, **100**, 219–226.
19. Bogenhagen,D.F., Martin,D.W. and Koller,A. (2014) Initial steps in RNA processing and ribosome assembly occur at mitochondrial DNA nucleoids. *Cell Metab.*, **19**, 618–629.
20. Rajala,N., Hensen,F., Wessels,H.J., Ives,D., Gloerich,J. and Spelbrink,J.N. (2015) Whole cell formaldehyde cross-linking simplifies purification of mitochondrial nucleoids and associated proteins involved in mitochondrial gene expression. *PLoS One*, **10**, e0116726.
21. Castello,A., Fischer,B., Eichelbaum,K., Horos,R., Beckmann,B.M., Strein,C., Davey,N.E., Humphreys,D.T., Preiss,T., Steinmetz,L.M. *et al.* (2012) Insights into RNA biology from an atlas of mammalian mRNA-binding proteins. *Cell*, **149**, 1393–1406.
22. Baltz,A.G., Munschauer,M., Schwanhausser,B., Vasile,A., Murakawa,Y., Schueler,M., Youngs,N., Penfold-Brown,D., Drew,K., Milek,M. *et al.* (2012) The mRNA-bound proteome and its global occupancy profile on protein-coding transcripts. *Mol. Cell*, **46**, 674–690.
23. Han,S., Udeshi,N.D., Deerinck,T.J., Svinkina,T., Ellisman,M.H., Carr,S.A. and Ting,A.Y. (2017) Proximity biotinylation as a method for mapping proteins associated with mtDNA in living cells. *Cell Chem. Biol.*, **24**, 404–414.
24. Ruhanen,H., Borrie,S., Szabadkai,G., Tyynismaa,H., Jones,A.W., Kang,D., Taanman,J.W. and Yasukawa,T. (2010) Mitochondrial single-stranded DNA binding protein is required for maintenance of mitochondrial DNA and 7S DNA but is not required for mitochondrial nucleoid organisation. *Biochim. Biophys. Acta*, **1803**, 931–939.
25. Milenkovic,D., Matic,S., Kuhl,I., Ruzzenente,B., Freyer,C., Jemt,E., Park,C.B., Falkenberg,M. and Larsson,N.G. (2013) TWINKLE is an essential mitochondrial helicase required for synthesis of nascent D-loop strands and complete mtDNA replication. *Hum. Mol. Genet.*, **22**, 1983–1993.
26. Spelbrink,J.N., Li,F.Y., Tiranti,V., Nikali,K., Yuan,Q.P., Tariq,M., Wanrooij,S., Garrido,N., Comi,G., Morandi,L. *et al.* (2001) Human mitochondrial DNA deletions associated with mutations in the gene encoding Twinkle, a phage T7 gene 4-like protein localized in mitochondria. *Nat. Genet.*, **28**, 223–231.
27. Tsien,R.Y. (1998) The green fluorescent protein. *Ann. Rev. Biochem.*, **67**, 509–544.
28. Fernandez-Millan,P., Lazaro,M., Cansiz-Arda,S., Gerhold,J.M., Rajala,N., Schmitz,C.A., Silva-Espina,C., Gil,D., Bernado,P., Valle,M. *et al.* (2015) The hexameric structure of the human mitochondrial replicative helicase Twinkle. *Nucleic Acids Res.*, **43**, 4284–4295.
29. Ziebarth,T.D., Gonzalez-Soltero,R., Makowska-Grzyska,M.M., Nunez-Ramirez,R., Carazo,J.M. and Kaguni,L.S. (2010) Dynamic effects of cofactors and DNA on the oligomeric state of human mitochondrial DNA helicase. *J. Biol. Chem.*, **285**, 14639–14647.
30. Rackham,O., Shearwood,A.M., Mercer,T.R., Davies,S.M., Mattick,J.S. and Filipovska,A. (2011) Long noncoding RNAs are generated from the mitochondrial genome and regulated by nuclear-encoded proteins. *RNA*, **17**, 2085–2093.
31. Antonicka,H. and Shoubridge,E.A. (2015) Mitochondrial RNA granules are centers for posttranscriptional RNA processing and ribosome biogenesis. *Cell Rep.*, **10**, 920–932.
32. Jourdain,A.A., Koppen,M., Rodley,C.D., Maundrell,K., Gueguen,N., Reynier,P., Guaras,A.M., Enriquez,J.A., Anderson,P., Simarro,M. *et al.* (2015) A mitochondria-specific isoform of FASTK is present in mitochondrial RNA granules and regulates gene expression and function. *Cell Rep.*, **10**, 1110–1121.
33. Popow,J., Alleaume,A.M., Curk,T., Schwarzl,T., Sauer,S. and Hentze,M.W. (2015) FASTKD2 is an RNA-binding protein required for mitochondrial RNA processing and translation. *RNA*, **21**, 1873–1884.
34. Pietras,Z., Wojcik,M.A., Borowski,L.S., Szewczyk,M., Kulinski,T.M., Cysewski,D., Stepien,P.P., Dziembowski,A. and Szczesny,R.J. (2018) Dedicated surveillance mechanism controls G-quadruplex forming non-coding RNAs in human mitochondria. *Nat. Commun.*, **9**, 2558.
35. Silva,S., Camino,L.P. and Aguilera,A. (2018) Human mitochondrial degradosome prevents harmful mitochondrial R loops and mitochondrial genome instability. *Proc. Natl. Acad. Sci. U.S.A.*, **115**, 11024–11029.
36. Chatre,L. and Ricchetti,M. (2013) Large heterogeneity of mitochondrial DNA transcription and initiation of replication exposed by single-cell imaging. *J. Cell Sci.*, **126**, 914–926.
37. Clemente,P., Pajak,A., Laine,I., Wibom,R., Wedell,A., Freyer,C. and Wredenberg,A. (2015) SUV3 helicase is required for correct processing of mitochondrial transcripts. *Nucleic Acids Res.*, **43**, 7398–7413.
38. Tu,Y.T. and Barrientos,A. (2015) The human mitochondrial DEAD-Box protein DDX28 resides in RNA granules and functions in mitoribosome assembly. *Cell Rep.*, **10**, 854–864.
39. Bogenhagen,D.F., Ostermeyer-Fay,A.G., Haley,J.D. and Garcia-Diaz,M. (2018) Kinetics and mechanism of mammalian mitochondrial ribosome assembly. *Cell Rep.*, **22**, 1935–1944.
40. Rosa,I.D., Durigon,R., Pearce,S.F., Rorbach,J., Hirst,E.M., Vidoni,S., Reyes,A., Brea-Calvo,G., Minczuk,M., Woellhaf,M.W. *et al.* (2014) MPV17L2 is required for ribosome assembly in mitochondria. *Nucleic Acids Res.*, **42**, 8500–8515.
41. Kehrein,K., Schilling,R., Moller-Hergt,B.V., Wurm,C.A., Jakobs,S., Lamkemeyer,T., Langer,T. and Ott,M. (2015) Organization of mitochondrial gene expression in two distinct Ribosome-Containing assemblies. *Cell Rep.* **10**, 843–853.
42. Morino,H., Pierce,S.B., Matsuda,Y., Walsh,T., Ohsawa,R., Newby,M., Hiraki-Kamon,K., Kuramochi,M., Lee,M.K., Klevit,R.E. *et al.* (2014) Mutations in Twinkle primase-helicase cause Perrault syndrome with neurologic features. *Neurol*, **83**, 2054–2061.
43. Chatzispyrou,I.A., Alders,M., Guerrero-Castillo,S., Zapata Perez,R., Haagmans,M.A., Mouchiroud,L., Koster,J., Ofman,R., Baas,F., Waterham,H.R. *et al.* (2017) A homozygous missense mutation in ERAL1, encoding a mitochondrial rRNA chaperone, causes Perrault syndrome. *Hum. Mol. Genet.*, **26**, 2541–2550.
44. Demain,L.A., Urquhart,J.E., O'Sullivan,J., Williams,S.G., Bhaskar,S.S., Jenkinson,E.M., Lourenco,C.M., Heiberg,A., Pearce,S.H., Shalev,S.A. *et al.* (2017) Expanding the genotypic spectrum of Perrault syndrome. *Clin. Genet.*, **91**, 302–312.